Data Analysis and Advanced Algorithms for Long-range Ultrasound Signal Processing

Ana Rita Diogo
Mestrado em Engenharia Física
Departamento de Física e Astronomia da Faculdade de Ciências da Universidade do Porto
2022

Supervisor
Prof. Dr. João Manuel R. S. Tavares, Faculdade de Engenharia da Universidade do Porto.

Co-supervisor
Dr. Carlos Avelino De Jesus Gouveia, EQS Global.

U.PORTO

FACULDADE DE CIÊNCIAS
UNIVERSIDADE DO PORTO

Todas as correções determinadas pelo júri, e só essas, foram efetuadas.

O Presidente do Júri,

Porto, ______/______/________

MSc

Sworn Statement

I, Ana Rita Inácio Fraga Diogo enrolled in the Master Degree in Engineering Physics at the Faculty of Sciences of the University of Porto hereby declare, in accordance with the provisions of paragraph a) of Article 14 of the Code of Ethical Conduct of the University of Porto, that the content of this internship report reflects perspectives, research work and my own interpretations at the time of its submission.

By submitting this internship report, I also declare that it contains the results of my own research work and contributions that have not been previously submitted to this or any other institution.

I further declare that all references to other authors fully comply with the rules of attribution and are referenced in the text by citation and identified in the bibliographic references section. This internship report does not include any content whose reproduction is protected by copyright laws.

I am aware that the practice of plagiarism and self-plagiarism constitute a form of academic offense.

Ana Rita Diogo

January 6, 2023

UNIVERSIDADE DO PORTO

MASTERS THESIS

Data Analysis and Advanced Algorithms for Long-range Ultrasound Signal Processing

Author:

Ana Rita DIOGO

Supervisor:

João Manuel R.S. TAVARES

Co-supervisor:

Carlos GOUVEIA

A thesis submitted in fulfilment of the requirements for the degree of MSc. Engineering Physics

at the

Faculdade de Ciências da Universidade do Porto
Departamento de Física e Astronomia

September 30, 2022

UNIVERSIDADE DO PORTO

Abstract

Faculdade de Ciências da Universidade do Porto
Departamento de Física e Astronomia

MSc. Engineering Physics

Data Analysis and Advanced Algorithms for Long-range Ultrasound Signal Processing

by Ana Rita DIOGO

Ultrasonic guided wave testing (UGWT) is a non-destructive testing (NDT) technique commonly used in structural health monitoring to perform wide-range inspection from a single point, thus reducing the time and effort required for NDT. However, the multi-modal and dispersive nature of guided waves makes the extraction of essential information that leads to defect detection an extremely challenging task. The goal of this internship was to study some of these algorithms and proceed to their implementation and evaluation to detect features and eventual defects in cylindrical structures.

An extensive study on various signal processing techniques was carried out as part of the literature review to choose the algorithm to implement throughout the internship. This review compared signal processing approaches to ultrasonic guided wave signals in different geometries, resulting in a published article.

The Split Spectrum Processing method was implemented and applied to several signals to detect features. The filter bank parameters were studied to find the optimum values correlated to the pipe structure analysed, as well as the different recombination algorithms. The ideal filter bank parameters were selected through a search brute force algorithm and the best results were obtained for the polarity threshold and polarity threshold with minimisation algorithms, in accordance with the literature.

Dispersive modes were first simulated to corroborate the method and results were found to follow the initial ones in the implementation phase. To validate the technique experimentally, several signals acquired through different techniques at frequencies of 60 kHz and 70 kHz, were propagated along a pipe structure containing features like welds and defects. The original signals were also reconstructed based on the results from the recombination algorithms, having the best results been obtained again for the polarity threshold and polarity threshold with minimisation, with SNR enhancement values of 37 dB and 35 dB, respectively. The improvement of choosing the best bank filter parameters, testing on more field data under varied conditions, and flaws should be the main areas of focus in future research on this topic, as well as the automation using machine learning techniques in order to fit it to the signal being studied.

Keywords: ultrasonic guided wave testing, data science, data analysis, signal processing, split spectrum processing.

UNIVERSIDADE DO PORTO

Resumo

Faculdade de Ciências da Universidade do Porto

Departamento de Física e Astronomia

Mestrado em Engenharia Física

Análise de Dados E Algoritmos Avançados para Processamento de Sinais de Ultrassons de Longo Alcance

por Ana Rita DIOGO

A testagem de ondas guiadas ultrassónicas (UGWT) é uma técnica de teste não destrutiva (NDT) geralmente usada em monitorização de integridade estrutural para realizar inspeção de longo alcance a partir de um único ponto, reduzindo assim o tempo e esforço necessário para NDT. No entanto, a natureza multimodal e dispersiva das ondas guiadas torna a extração de informação essencial que leva à deteção de defeitos uma tarefa extremamente complicada. O objetivo deste estágio foi estudar alguns destes algoritmos e proceder à sua implementação e avaliação para detetar características e eventuais defeitos em estruturas cilíndricas.

Foi realizado um estudo extensivo sobre várias técnicas de processamento de sinal como parte da revisão de literatura para escolher o algoritmo a ser implementado ao longo do estágio. Esta revisão comparou abordagens de processamento de sinal para sinais de ondas guiadas por ultrassom em diferentes geometrias, resultando num artigo publicado.

Foi implementado o método *Split Spectrum Processing* e aplicado a diversos sinais para detetar características. Os parâmetros do banco de filtros foram estudados a fim de encontrar os valores ótimos correlacionados com a tubagem analisada, bem como os diferentes algoritmos de recombinação. Os parâmetros do banco de filtros ideais foram selecionados por meio de um algoritmo de busca de força bruta e os melhores resultados foram obtidos para os algoritmos *polarity threshold* e *polarity threshold with minimisation*, de acordo com a literatura.

Os modos dispersivos foram inicialmente simulados para corroborar o método e os resultados encontrados seguem os iniciais na fase de implementação. Para validar a técnica experimentalmente, vários sinais adquiridos através de diferentes técnicas nas frequências de 60 kHz e 70 kHz, foram propagados ao longo de uma estrutura de tubagem contendo características como soldas e defeitos. Os sinais originais também foram reconstruídos com base nos resultados dos algoritmos de recombinação, tendo os melhores resultados sido obtidos novamente para o *polarity threshold* e *polarity threshold with minimisation*, com valores de melhoria de SNR de 37 dB e 35 dB, respetivamente. A melhoria da escolha dos parâmetros ótimos do banco de filtros, testes em mais dados de campo sob condições e falhas variadas devem ser as principais áreas de foco em trabalhos futuros sobre este tema, assim como a automação utilizando técnicas de *machine learning* para adequá-lo a o sinal estudado.

Palavras-chave: testagem de ondas guiadas ultrassónicas, ciência dos dados, análise de dados, processamento de sinal, *split spectrum processing*.

Contents

List of Figures

List of Tables

Glossary

UGWT	Ultrasonic guided wave testing
UT	Ultrasonic testing
EMAT	Electromagnetic acoustic transducer
SNR	Signal-to-noise ratio
NLMS	Normalised least mean square
WT	Wavelet transform
SDMP	Dispersion based matching pursuit
EMD	Empirical mode decomposition
CSA	Cross-sectional area
SSP	Split spectrum
SH	Shear horizontal
MUSIC	Multiple Signal Classification
ESPRIT	Estimation of signal parameters via rotational variant technique
PSO	Particle swarm optimization
ST-SWA	Spatio-temporal sparse wavenumber analysis
NDT	Non-destructive testing
NDE	Non-destructive evaluation
RAPID	Reconstruction algorithm for the probabilistic inspection of damage
CFRP	Carbon fiber reinforced polymer
RTM	Reverse-time migration
EFIT	Elastodynamic finite integration technique

MLS	Maximum Length Sequence
DCNN	Deep convolutional neural network
WRS	Weight-range selection
FFT	Fast Fourier transform
MOT	Magneto-optical transducer
STFT	Short-time Fourier transform

Chapter 1

Introduction

1.1 Context

Tanks, pressure vessels and pipelines are omnipresent infrastructures in the industry, where they are used to store and transport products and raw materials to and from factories, and, in many cases, to distribution points and end customers. Over time, due to material ageing, corrosion will reduce the original wall thickness of these structures, which may compromise their reliable operation and even cause the collapse of the assets. In addition to representing, in many cases, risk to the environment, health and integrity of workers and surroundings populations; this type of situation can cause high economic losses, directly due to unscheduled stops and indirectly due to supply failures. Thus, within the scope of protection and optimisation of structural resilience of critical assets, it is fundamental to carry out inspection of structural integrity to follow the evolution of the structure condition during its ageing. In this context, ultrasonic guided waves testing (UGWT) has shown capabilities of surveying large structural components for defects, contrary to conventional Ultrasonic Testing (UT) based on punctual measurements, providing more comprehensive information about the integrity condition of the structure under analysis [1] (Figure 1.1). Moreover, UT allows for the detection of both internal and external flaws as well as the measurement of thickness and the detection of corrosion or erosion. When there is a discontinuity (like a fracture), some of the delivered sound energy is reflected in the cracked surface as waves that travel through the materials. The wave signal is then converted by the transducer into an electrical signal that can be analysed.

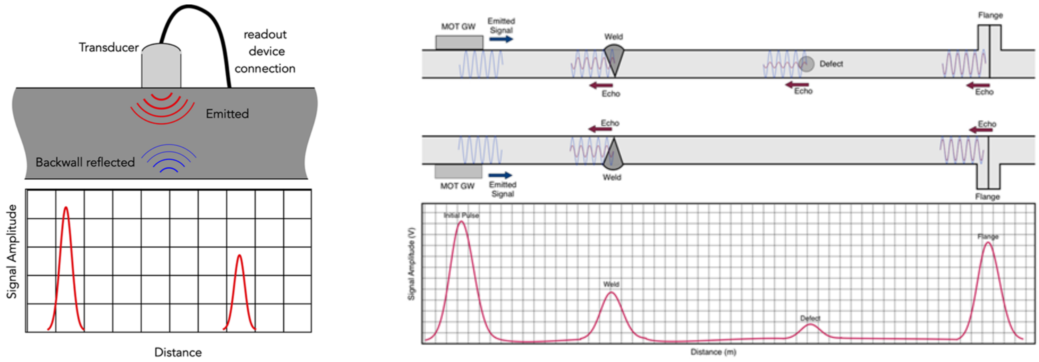

FIGURE 1.1: Representation of the conceptual difference between conventional ultrasonic testing (left) and guided wave ultrasonic testing (right) [2]

Guided waves are elastic waves generated directly in the structure under analysis, which propagate along its length, confined by the geometric limits of its walls. Hence, they propagate through the structure and are reflected by variations in the wall cross-section. The indications obtained may be related to geometric changes and variations in thickness [1]. Using the arrival time of echoes and propagation velocity in the medium, it is possible to determine the position of these changes. In turn, the amplitude of the signals allows for the estimation of defect sizes [3]. Thus, this technique makes it possible to locate internal or external defects along an in-service pipe at distances of a few tens of meters from a single excitation point. Moreover, it is possible to evaluate underground and coated or isolated structures without the need to alter them, providing more comprehensive information about the integrity condition of the structure under analysis.

Unlike conventional UT, there are an infinite number of guided wave modes that are supported by a structure. Depending on the geometry of the structure, these modes follow a certain classification. For plates, there are two families of modes: the Lamb waves (Symmetric and Asymmetric) and the Shear Horizontal waves. On the other hand, for cylindrical geometries, modes can be grouped into three families, namely the Torsional, Longitudinal and Flexural modes. The acoustic properties of wave modes are a function of the wall thickness, the material and the frequency. Predicting the properties of the wave modes often relies on heavy mathematical modelling which is typically presented in graphical plots called dispersion curves. Dispersion is the variation of phase and group velocities of the ultrasonic guided signal and its propagation characteristics with the frequency and thickness of the material. Thereby, the dispersion curves represent the velocities for each mode as a function of frequency. Most wave modes are dispersive, i.e., the velocity varies with frequency. Dispersion causes the wave-packets to spread out in time as they propagate through a structure. Only Torsional and Shear Horizontal waves are non-dispersive, and therefore are preferred for generation [4].

1.2 Problem statement

In UGWT, the generation and detection of these signals are done using a transducer mechanically coupled to the structure under analysis. There are three main technologies for these transducers:

- Piezoelectric: transducers able to convert mechanical strain from electrical voltage and vice versa. To create a variable electric field that operates on the material, this device uses a piezoelectric material sandwiched between two electrodes. Due to its characteristics, it compresses and relaxes based on how strong the applied electric field is. Since an acoustic wave is formed in the ultrasound area, a structure can transmit an acoustic wave there very well. This kind of device can be applied to a variety of surfaces, but it needs good contact with the surface being studied. It does, however, have certain limitations, like the efficiency decreasing with temperature, the need for a coupling agent that is temperature sensitive, and the need for the best coupling with the material to be studied.

- EMAT (Electromagnetic Acoustic Transducer): it uses the interaction between a magnetic field and the properties of the material under study to generate or detect acoustic waves. It is made up of a permanent magnet, a transducer substance, and a coil where the alternating current is induced. Thus, the Lorentz force and the magnetostrictive force appear within the sample as a result of the interaction between the static magnetic field and the dynamic magnetic field. Depending on the configuration, different kinds of ultrasonic waves can be produced. The main benefit of this device is that it doesn't need mechanical contact with the surface of the material being studied (Figure 1.2).

- Magnetostrictive: utilises a specific kind of magnetic material in which an oscillating magnetic field is applied to compress the atoms of the material together, causing a periodic change in the material's length and a high-frequency mechanical vibration as a result. Due to their suitability for temperatures up to 600°C and the fact that they can be used in contact or contactless approach with the material being studied, magnetostrictive transducers are typically used in the lower frequency ranges and are frequently used in ultrasonic cleaners and ultrasonic machining applications. Additionally, they have a signal one order of magnitude stronger than an EMAT.

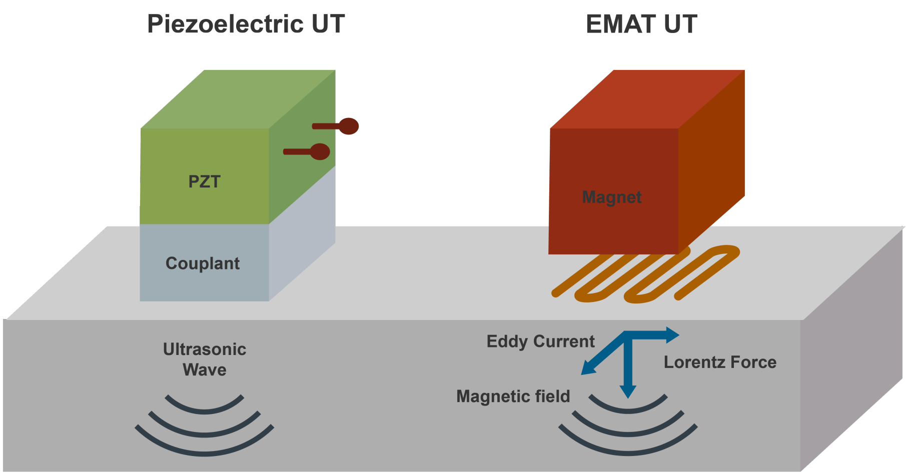

FIGURE 1.2: Comparison between the piezoelectric transducer (left) and EMAT (right) for generation of ultrasonic waves.

For instance, in pipes, the transducer is a collar consisting of an array of piezoelectric elements where the elements are excited equally and simultaneously in order to generate an axis-symmetric wave [3]. Alternatively, a 360º magnetostrictive ring transducer can be used and, in this case, the axis-symmetric generation is ensured due to the symmetry of the patch. In both cases, as stated before, the Torsional waves, in particular their fundamental mode, are commonly used as excitation waves due to their properties. Nevertheless, even generating non-dispersive waves with axial symmetry, the non-symmetric nature of defects and some construction features of the structures will cause mode conversion and give rise to dispersive signals. The presence of dispersive waves in the signals is also seen as coherent noise. Coherent noise, as its name indicates, cannot be eliminated by averaging as it is not random. On the other hand, as it coincides in frequency with the signal of interest, it cannot be filtered using conventional filtering techniques. The piezoelectric transducers acquire signals that suffer less from the effect of dispersion, so their SNR is higher. However, this type of device presents limitations in terms of the distance of inspection. This distance is much greater from magnetostrictive devices.

The multi-modal and dispersive nature of guided waves makes signal processing particularly challenging, which has been the subject of several studies over the years [5–7]. These techniques are necessary not only for the interpretation of the received ultrasonic signals but also for procedure automation, which improves non-destructive testing and evaluation, along with the reliability and replicability of the process. Some of the issues that stem from this involve the elimination of dispersive modes, mode separation and defect identification, as well as their classification. To enhance and improve the detection and classification of defects, several methods have been employed to process the input signal such as time-frequency representation (including the reassigned spectrogram and the Wigner-Ville distribution), wavelet analysis, Hilbert-Huang transforms and cross-correlation techniques [8–12].

1.3 Objectives

The internship has been developed at EQS Global, a company that provides specialised services and digital solutions to help businesses manage their assets and operations, guaranteeing quality, compliance, improving reliability, performance and preventing incidents from happening. The main goal is to apply advanced signal processing algorithms to minimise the effect of dispersion and thus improve data analysis for UGWT using magnetostrictive transducers.

1.4 Scientific Contribution

The removal and separation of dispersive modes from a UGW signal have been subject to various studies over the years and while progress has been made, there is still room for improvement as new techniques are constantly being developed. To understand the problem at hand and determine the best approach in terms of signal processing techniques, an extensive review of articles published in the last 20 years on signal processing of ultrasonic guided wave signals was carried out. The results of the study are presented in the next chapter and resulted in a published article.

1.5 Report structure

The following report is divided into five chapters to assist its reading and present the information in a clear and organised manner. In this first chapter, an introduction to the context of the project is provided, along with the motivation and problem statement. The second chapter provides an overview of the current state of the art, in which the research is detailed, and signal processing techniques are reviewed according to their purpose and geometry of the structure under analysis, describing the advantages and limitations of each technique. The third chapter describes the methods used during the internship, outlining the complete process from conceptualisation to implementation. Results obtained are discussed in the fourth chapter where they are critically analysed and interpreted, as well as the optimisation of the methods. The final chapter provides conclusions and suggestions for further work, followed by the bibliography.

Chapter 2

Literature Review

2.1 Searching methods

A systematic review was performed in the SCOPUS database using the following keywords: ”signal processing” and ”ultrasonic guided wave testing”, yielding 251 unique results (Figure 2.1). Based on an analysis of the title and abstract, 177 works were excluded for not meeting the following inclusion criteria: using signal processing algorithms and being suitable for ultrasonic guided wave testing. Of the selected results, all conference proceedings and book chapters were excluded, as well as 3 literature reviews, which are detailed in the next sections. Further analysis of the body of text was done, leaving 51 full-text original studies which propose signal processing techniques and algorithms for ultrasonic guided wave testing in metallic structures. The PRISMA diagram of the performed systematic search can be seen below (Figure 2.2).

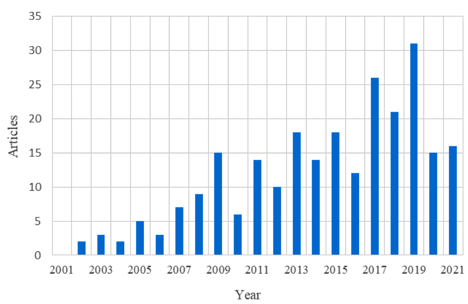

FIGURE 2.1: Articles with the keywords ”guided wave ultrasonic testing, signal processing” published in the last 20 years.

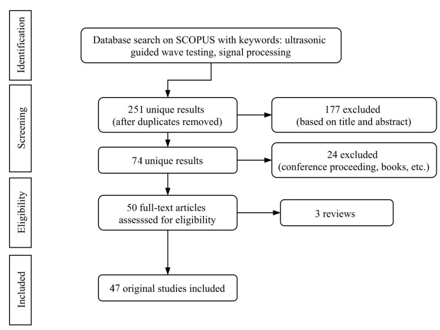

FIGURE 2.2: PRISMA study flow diagram of the performed systematic literature review.

2.2 Signal processing techniques

As aforementioned, the processing of the guided wave signals resulting from the interference of the multiple modes supported by the structure under analysis, to gather information about its integrity, is still an important challenge in UGWT. Over the last decade, several techniques have been developed and tested for distinct purposes. Various articles focus on filtering (removal) dispersive modes in order to improve the signal-to-noise ratio (SNR) and consequently increase the sensitivity for defect detection [13–16]. Also, filtering dispersive modes improves the accuracy of damage localisation by the increase of the spatial resolution, as Moll *et al.* demonstrated by employing a time-varying inverse filter to convert them into broad-band high-resolution signals [17]. However, removing these modes can also imply the loss of relevant information: these modes carry relevant details regarding the nature of the defects, for example, angular position and if it is external or internal [18]. Thereby, the ability to separate modes rather than eliminate the dispersive ones is quite appealing [7, 19]. Beyond signal enhancement and wave mode isolation, the identification and localisation of the defects are also critical factors in UGWT. Damage identification and classification have also been explored in several works [20–24], not only to roughly locate them but also to assess their dimensions and to discern between the types of defects. At last, a new tendency that has been expanding is the use of machine learning which, when combined with signal processing, allows for improved new methods in terms of identification and classification of damage [25, 26]. It is important to note the application of these signal processing techniques depends on the geometry of the structure under analysis as well as their advantages and limitations. An overview is presented in the next sections, where the main used techniques are described.

2.2.1 Pipes

Non-destructive testing and evaluation have become an important approach to reducing losses and saving inspection time, specifically in pipelines, which are prevalent in all industries as part of transportation and distribution networks [27]. Pipes are usually modelled as hollow cylinders, where axial propagation consists of Torsional and Longitudinal modes. In these structures, three types of modes are admitted: Torsional mode $T(0,m)$, Longitudinal axisymmetric mode $L(0,m)$ and Flexural asymmetrical mode $F(n, m)$, where n is the circumferential order, and m is a variable used to distinguish the modes of a given order n [28]. Some of the most prominent issues that signal processing techniques aim to solve when it comes to the structural health of pipelines include the improvement of signal-to-noise ratio through the cancellation of dispersive modes, isolation of modes and imaging of defects, as well as the characterisation of symmetric and asymmetric defects.

As stated before, dispersive modes decrease the SNR and the spatial resolution; thus, decreasing the sensitivity of the solution to detect defects and hindering the ability to distinguish between defects close to each other or close to a construction feature of the structure under analysis, such as welding and bolts. The elimination or filtering of these specific modes is of great relevance in terms of signal processing, which can be achieved with the use of methods such as dispersion compensation, compressed pulse analysis and split spectrum processing. Adaptive filtering was first introduced by Widrow *et al.* as a way to estimate signals distorted by noise or interference [29]. By making use of a primary input that contains the corrupted signal and a ”reference” input that contains noise correlated to the latter, in which the reference input is adaptively filtered and subtracted from the primary input. Mahal *et al.* proposed a new method to eliminate Flexural wave modes, instead of extracting noise from the single time-domain signal by utilising adaptive filtering. This technique, as mentioned before, is often utilised as an adaptive noise canceller and increases the SNR. Different adaption algorithms can be applied, but in this specific case, the authors have employed leaky normalised least mean square (NLMS), which is more suited for guided wave applications with time-varying noise because it decreases the amplification of gradient noise and also provides a fast rate of convergence (Figure 2.3).

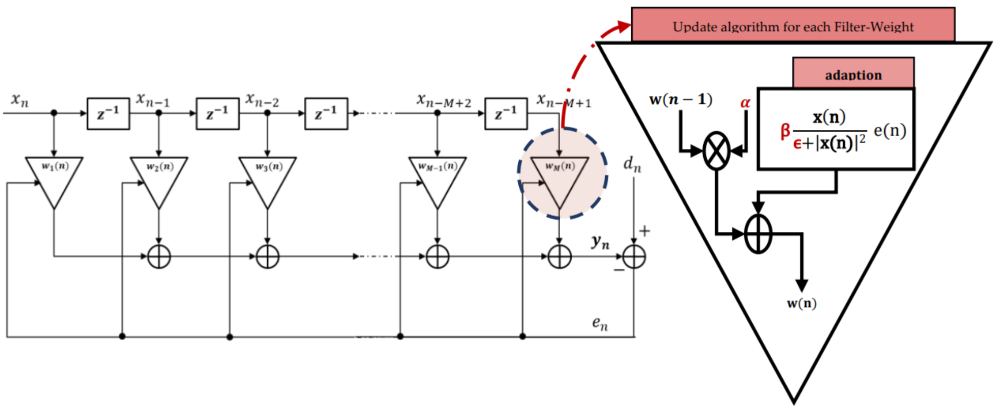

FIGURE 2.3: Adaptive linear prediction filter algorithm for noise cancellation where the red marked parameters are fixed [30].

The application of a leakage factor allows for a faster adaption of the filter weights to the existing noise of each iteration [30]. The optimal parameter selection is a trade-off between maximum gain and stable amplification of the SNR of smaller defects.

Furthermore, other techniques that have conventionally been explored for UT can be adapted to UGWT. Split spectrum processing was first applied with reference to surface search radar operation [31], having later been adapted to ultrasonic testing [32]. This technique, also known as signal sub-band decomposition, consists of five major components. First, the signal is to be converted from time-domain to frequency-domain, followed by the implementation of a bank of band-pass filters that splits the signal into a set of sub-bands at different centre frequencies. The results are then converted back to time-domain, where each element is normalised by a weighting factor and finally assembled through a recombination algorithm to yield the output filtered signal. The various frequency signals in ultrasound are produced by dividing the frequency spectrum of the received signal, rather than transmitting at different frequencies, as is the case in radar applications, and are not correlated with each other. As a result, when these diverse frequency signals are composited using various algorithms, the SNR can be improved. The success of this technique is however dependent on the selection of the filter bank parameters. Good results have previously been achieved for UT testing, but the same values were not found to be appropriate for UGWT, due to the existence of a combination of modes that operate in the kHz range with different velocities [33]. Using a brute force search algorithm to manage parameter selection, Pedram *et al.* made it possible to enhance the SNR and spatial resolution of ultrasonic guided wave signals by removing dispersive wave modes, a method which has since then been improved as a post-processing approach on coated pipes to reduce the attenuation effects [34].

Mahal *et al.* introduced a novel statistical approach to identifying defect signals corrupted by coherent noise by utilising the full potential of the tool-set array of conventional guided waves inspection devices. This technique demonstrates the capability of detecting defects utilising all of the individual transducers rather than a single signal obtained after the general process. Three different methods were tested: the first, where the threshold value is static and defined by the inspector, produced the worst results and in the second the assigned threshold to each iteration is a percentage taken from the summation of the amplitude of all of the transducers signals as the time-domain signal generated by the normal propagation routine. In the third one, the number of transducers with the same phase over the total number of transducers, subtracted by an offset determines the percentage value, which yielded similar results to the second method, but the threshold value can be set automatically, providing a great benefit in one-off inspections. This technique also allows the possibility of developing narrowband transducers, as opposed to the currently used wideband transducers, which have a more focused transfer function and stronger excitation power [35].

However essential increasing the SNR of a signal may be, it does have a downside, since dispersive modes carry important information regarding the characteristics of existing damage. Preserving this type of information through the isolation and separation of modes instead of its filtering becomes then an attractive approach. This can be achieved through several methods, such as applying a wavelet transform (WT) which decomposes a function into a set of wavelets, allowing the extraction of local spectral and temporal information simultaneously [5, 20]. This concept was first developed by Haar, and since then has been extensively studied [36]. Nevertheless, the improper selection of the mother wavelet will significantly affect the usefulness of this method in extracting defect information from the reflected signals. It has also been shown not to be suitable for the reduction of coherent noise, as it removes the smaller amplitudes regardless of whether they are signal or noise, an issue also found in the application of cross-correlation techniques. Chen J. further proposed the use of the tone-burst wavelet as the mother wavelet to denoise the signal, which was found to be effective in extracting the defect-related signals and obtaining better results when compared to the conventional Morlet wavelet, by comparing the temporal waveforms of the normal pipe with those of the corroded pipe [37].

Matching pursuit is a technique often used to separate overlapped modes, that finds the best match for a signal from an over-complete and redundant dictionary and has the advantage of being applicable to any type of structure, given the proper dictionary. Matching pursuit decomposition is commonly used to find discrete echoes in a signal, but it can also be thought of as providing distinctive wavelets that reflect areas of the signal where energy is concentrated in complex signals [38]. The main limitation of this method comes down to the construction of the dictionaries, as it is difficult and time-consuming to collect extensive data for that end. This technique has been combined with others to enhance damage detection. A differential evolution algorithm has been employed to improve parameter searching efficiency, and cross-term free time-frequency distribution is achieved by superimposing the Wigner-Ville distribution of each matching atom decomposed [24]. The Gaussian modulated functions were chosen as matching atoms because their time-frequency characteristics match ultrasonic guided-wave signals effectively. The effectiveness of parameter searches can be considerably improved by using the differential evolution technique, and flaws can be distinguished from echo signals using time-frequency distribution characteristic comparison. The Wigner-Ville distribution function was first proposed by Eugene Wigner when making calculations of the quantum corrections to classical statistical mechanics and was later derived as a quadratic representation of the local time-frequency energy of a signal by J. Ville [39]. Rostami J. *et al.* expanded upon this by proposing sparse representation with dispersion based matching pursuit (SDMP), which takes dispersion into account, increasing the sparsity of the final representation [7]. This technique consists of a two-stage algorithm, designed with a dictionary based on actual waves obtained from finite element simulations, to represent guided wave signals with the maximum sparsity. In the first stage, a signal is approximated and in the second, sparsity is further increased based on the frequency components of the excitation signal. Thus, undesired components of guided wave signals are filtered and at the end, a very clean signal with meaningfully decomposed components remains for further analysis. This method can be extended to any plate-like structure made from different materials such as plastic pipes, aluminum and composite plates, steel strands and rails, on the condition that a new dictionary is designed with reference to the geometry of the structure and its material.

To detect and determine the localisation of defects, Mahal H. *et al.* proposed a condition-based comparison of the power spectrum achieved from a sliding moving window for the received signal. The algorithm consists of several steps, the first being its initialisation, which initialises the excitation sequence to extract the necessary features for analysis. Then the main loop uses the advancing window and carries out the pre- and post-processing of the conditions. Finally, the spectrum of each iteration is compared with the one achieved from the excitation sequence. In each iteration, the signal is normalised, and its corresponding power spectrum is generated to detect the Torsional wave. However, due to significant changes in the excitation sequences, it is not recommended to use this algorithm with frequencies higher than 42 kHz [6].

With the growth of the machine learning field, new signal processing methods are being integrated with these algorithms. Artificial neural networks, for example, are very appealing due to their ability of generalisation and for the characteristic of not requiring any fault physical model. Cau *et al.* made use of traditional feed-forward multi-layer perceptron networks to obtain information on the size and location of notches. The study employs Torsional waves as excitation waves and the finite element method has been used to model pipes and defects to obtain several echoes containing damage information. The obtained signals were then processed to reduce the dimension and extract relevant features. Preliminary results show that the return time of the received signals is linearly dependent on the defect position while independent of the entity of the fault, so the notch position can therefore be determined with accuracy [25]. On the other hand, the correlation between the variation in time-frequency spectra and the shift in predominant modes with the spread of corrosion can be obtained from the deduction of the dispersion curves. To track the mode conversions as corrosion progressed, a new time-frequency spectrum was constructed. By employing the k-means clustering method, indices have been used to quantify the change in signal intensity with the progress of corrosion along with a modified S-transform. The subjectivity of contact type monitoring paradigms to contact pressure is a common source of uncertainty. The proposed method addressed this issue by processing signals time-frequency-based, with the key components based on propagating modes rather than signal amplitudes [40].

Author	Year	Technique	Summary and results
Liu S. [5]	2021	Wavelet transform (WT) and empirical mode decomposition (EMD)	The decomposed signal in WT can better preserve defect information and reduce the interference of noise signals, but the signal processed by the EMD is better than that of the WT.
Chen J. [37]	2017	Tone-burst wavelet	Results show that the location of the corroded areas of the pipes could be accurately detected using the calculated group velocity of the guided wave. Comparing the temporal waveforms of the normal pipe with those of the corrosion, flaws were easily observed and detected.
Rostami J. [7]	2017	Sparse Representation with Dispersion Based Matching Pursuit	The SDMP with dispersive dictionary has greatly enhanced the performance of matching pursuit and guarantees the maximum sparsity. Although the presented SDMP for signal interpretation addresses the inspection of steel pipes, it can be applied to any plate.
Mahal H. [6]	2019	Sliding moving window	Three different pipes with defects sizes of 4, 3 and 2% cross-sectional area (CSA) material loss were evaluated. Results demonstrate the capability of this algorithm in detecting Torsional waves with low SNR without requiring any change in the excitation sequence.
Pedram S. [33]	2018	Split-spectrum processing	Both techniques achieved the greatest SNR without distorting the relative amplitudes of the signal of interest where an improvement of up to 38.9 dB was observed. SSP shows good potential to increase the inspection range from a single test location as it significantly reduces the level of coherent noise.

TABLE 2.1: Works found addressing signal processing techniques applied to pipes.

Author	Year	Technique	Summary and results
Pedram S. [34]	2020	Split-spectrum processing	SSP algorithm is shown to have great potential to decrease the background noise entirely by minimising the effect of undesired wave modes throughout the signal's trace, whereas the traditional method was not able to do it. Good results were obtained for coated pipes.
Mahal H. [35]	2018	Axisymmetric wave detection algorithm	An axisymmetric wave detection algorithm was designed, which was validated by laboratory trials on real-pipe data with two defects on different locations with varying CSA sizes.
Mahal H. [30]	2019	Adaptive leaky NLMS filter	The results demonstrated the capability of this algorithm for enhancing the SNR of the defect. The results proved that the model parameters can be chosen using a finite element method model, but it will not result in the maximum gain.
Majhi S. [40]	2019	Modified S-Transform	A novel time-frequency spectrum was developed to monitor the mode conversions in relation to the progress of corrosion. K-means clustering is used to quantify the variation in signal strengths with progress of corrosion. The proposed technique was able to obtain the variation in distribution of spectral contribution from higher order to lower order modes.

TABLE 2.1: continued.

2.2.2 Plate-like structures

The planar geometry of plates differs from cylindrical pipes, and thus different approaches are required. Usually, planar based ultrasonic guided wave transducers are used for pressure vessels, tank bottom plates and wall inspection. Guided waves in plates depend on reflections from the upper and lower surfaces of the plates to travel long distances on the plate parallel to these surfaces. The profile and the velocity of each guided wave mode in plates depend uniquely on their frequency and thickness of the structure; hence, thinner plates may support guided waves with higher frequencies than thicker plates. There are two families of wave modes for plates: the Lamb Waves and the Shear Horizontal (SH) Waves. In the Lamb waves, the particle direction is parallel (longitudinal direction) to the wave propagation direction and normal to the plate, and there are two different subfamilies of modes: symmetrical (S) and asymmetrical (A). For the SH modes, the particle displacement is perpendicular to the wave propagation direction. The notation used for these modes is An, Sn and SHn, where n represents the order of the mode.

In terms of filtering dispersive modes and improving SNR, techniques such as wavelet transform based noise processing and compressed sensing methods can be employed. Ianni *et al.* accomplished to minimise the number of scan point locations over the surface of an inspected structure by using compressed sensing of full wave field data. This method asserts that thanks to sparsity, a signal can be acquired and recovered from a limited number of linear measurements without loss of information, being the reconstruction performance influenced at large by the choice of a suitable decomposition basis to exploit such sparsity [41]. Furthermore, wavelet transforms have also been previously mentioned and studied with the purpose of denoising, as Da *et al.* proposed two approaches to this issue, based on time and wavenumber domains, allowing for a successful inverse reconstruction of flaws by reflected signals with signal noise ratio as high as -5 dB [42].

When it comes to dispersion compensation, a MUSIC-based multichannel method was employed by Zabbal *et al.* to extract dispersion curves from experimental data [43]. When compared to single vector decomposition techniques, this method enhances weak modes and displays a low noise level and a high wavenumber resolution, allowing for the characterisation of multi-layered structures of different materials. Xu *et al.* carried out dispersion compensation as well for both single-mode and multi-mode guided waves by utilising the dispersion curves of the guided wave modes in order to sparsely decompose the recorded dispersive guided waves [44].

The use of estimation of signal parameters via rotation invariant technique (ESPRIT) and particle optimisation algorithm has been employed by Chen *et al.*, resulting in root mean squared errors between the estimated and theoretical dispersion curves calculated by the inversed model parameters for simulation, steel, aluminium and composite experiments are: 0.027, 0.032, 0.033 and 0.102 rad/m [45]. The ESPRIT based dispersion curves extraction strategy offers a sharp objective function in the parameter space, whereas the

PSO optimiser can be implemented with ease and a few parameters need to be tuned. The spatio-temporal sparse wavenumber analysis implemented by Sabeti *et al.* achieved good results as well for the extraction of dispersion curves, with results indicating the possibility of accurate reconstruction (correlation coefficient of around 0.9) for sampling rates above 60% of the spatio-temporal Nyquist critical sampling rate. ST-SWA takes a temporally and spatially under-sampled guided wave data matrix as input and retrieves the sparse representation of the wave field in the frequency-wavenumber domain using the two-dimensional model and two-dimensional sparse recovery techniques. The generated representation can then be fed into a forward problem by the model to rebuild the original fully sampled wave field [46]. The results indicate that as long as overfitting is avoided, minor improvements in reconstruction accuracies can be observed at greater sparsities.

Time-frequency methods allow for an analysis of acoustic signals with multiple propagation modes, as well as the measurement of group velocity dispersion. The dispersion of several Lamb modes over a wide frequency range can be calculated from a single measurement by combining time-frequency analysis with a broadband acoustic excitation source [9]. As opposed to the Wigner-Ville distribution, the smoothed Wigner-Ville distribution offers a better representation of individual modes and can localise multiple closely-spaced modes in both time and frequency [10]. Wu *et al.* was able to successfully isolate guided wave modes with a signal decomposition algorithm, combining Smoothed Pseudo Wigner-Ville distribution to obtain the time-frequency distribution and Vold-Kalman filter order tracking to isolate modes. The location of defects can be obtained by the decomposition results. First, the Smoothed Pseudo Wigner-Ville Distribution processes the signal to get the corresponding time-frequency distribution, followed by the extraction and separation of the different modes. The Vold Kalman Filter Order Tracking is then applied to filter specific mode waveforms. A peak-track algorithm is then conducted in the significant areas and finally, to minimise error, a corresponding filter is built in time domain [19]. The technique can also be used in analogue NDT and NDE based on ultrasonic guided waves.

As previously stated, mode separation is quite an appealing approach to signal processing since it preserves the information contained in dispersive modes. Ratassepp *et al.* was able to perform this with a technique based on the guided wave mode orthogonality, used to separate the multi-modal signal into individual time-domain Lamb and SH mode components at the plate edge with successful results. In comparison to the standard spatial fast Fourier transform, the orthogonality-relation-based technique reduces the number of monitoring points and eliminates the need for additional mode filtering operations because obtaining the amplitudes of the modes is simple. Although the through-thickness displacements and stress field components must be measured, the orthogonality-relation at the plate edge is simplified because the stresses are null. As a result, only displacement components must be measured at a plate edge, making the method practicable [47].

Identifying distances and depth of damage is also a prevalent topic, and recent studies search to integrate machine learning to achieve better results. Rizvi *et al.* utilised an autoregressive model based on Burg's maximum entropy method to modify the kernel of the discrete Wigner-Ville distribution with an uncertainty of 5% [48]. The conventional Burg algorithm determines the reflection coefficient by minimizing the backward and forward prediction error of a single sequence or segment, but the Wael and Broersen algorithm is highly efficient in estimating the prediction error of all the segments taken together, hence a single model can be exploited for all the kernel sequences at a time. This model is more robust and stable, less biased, and more computationally efficient. The proposed technique can also be applied to pipes. It is important to mention that the current study used supervised machine learning to model the other dimensions of the crack. In a realistic case, these parameters would be unknown and would significantly affect the damage signal. Artificial neural networks have also been employed, where features extracted are fed to the network, enabling the classification of defects with a success rate $> 75\%$ [49]. Defect identification can also be done by using baseline methods, processing the signals and extracting the time parameters of the wave packets in mode conversion signals [50–52]. Deep learning has also been employed for this end [53].

Another approach commonly implemented makes use of image reconstruction to identify defects in the structure under analysis. He *et al.* proposed a multi-mode damage imaging technique which combines a reverse-time migration algorithm with a 3D wave propagation simulator with the potential to simultaneously determine damage type, size and location. Even though it wasn't possible to obtain detailed information on different modes, good results were achieved for damage location and defect size [54]. Furthermore, a reconstruction algorithm for probabilistic inspection of damage (RAPID) was utilised for tomography [55], with a more accurate quantitative visualisation obtained using the dominant mode, identified through frequency shifting and short-time Fourier transform

[56]. Image constructed from the correlation coefficients between the scattering signal and the atoms of the dictionary using a weighted sparse reconstruction-based anomaly imaging method yield accurate weights [57]. By using the appropriate weights applied to the objective function, the presented method can achieve anomaly imaging with fewer artefacts, making the success of this method limited to the selection of a suitable dictionary (Figure 2.4).

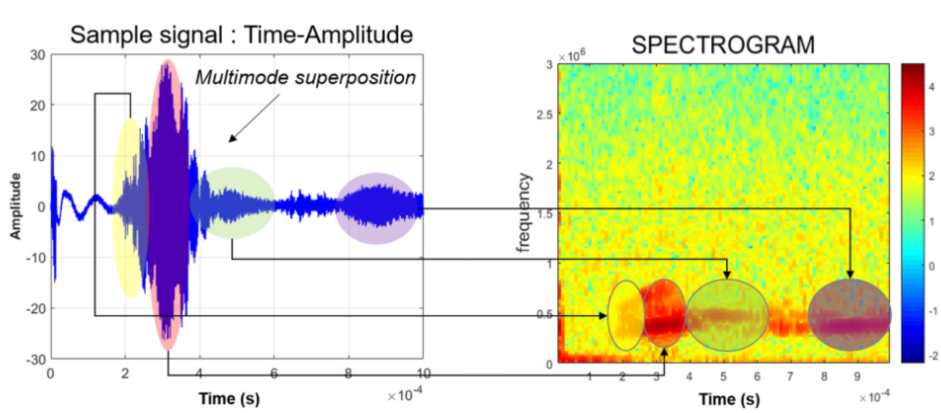

FIGURE 2.4: The mode identification process of Lamb waves considering group velocity, frequency, and superposition effect [56].

Zhang *et al.* developed a processing technique to separate modes to effectively remove the artefacts resulting from the multi-mode interference in the imaging process, able to properly measure multi-site faults with geometry, size, and depth information. Green's function is used to back-propagate the scattering Lamb signals in the frequency-domain, allowing the monitored area's back-propagated acoustic field information to be collected. A reverse-time migration method is then applied to reconstruct damage, by the cross-correlation between the incident acoustic field and the back-propagated acoustic field [58]. Numerical results show that mode separation pre-processing aids in effectively removing artefacts caused by multi-mode interference in the imaging process. Full waveform inversion algorithm is also an interesting guided wave tomography method, which makes use of a numerical forward model to predict the waveform of guided waves when propagating through corrosion defects and an inverse model to reconstruct the thickness map from the ultrasonic signals captured by transducers around the defect. Results by Rao *et al.* show that it is affected by the shape of the defect [59]. The abrupt change in the wall thickness has been shown to decrease the reconstruction error of small defects compared to the smoothly varying thickness.

Lugovtsova Y. *et al.* studied several wavenumber mapping techniques applied to composite-overwrapped pressure vessels. The study proposes the pre-processing of the wavefield so that only one mode at one frequency is left before wavenumber mapping, followed by the application of instantaneous and local wavenumber techniques. This method presents an excellent defect sensitivity and suitable defect quantification performance. The main limitation of this approach is that it is not possible to quantify every delamination between CFRP plies caused by the impact, as is the case for conventional UT. Only some parts of the impact damage are visible in the wavenumber and thickness maps. Another limitation is that the relation between wavenumber and effective thickness is non-monotonous, due to the complexity of the layup of the composite plate used in experiments and its anisotropy [60].

Wind turbines are often subject to guided wave testing since they are subjected to significant mechanical loads, necessitating an appropriate maintenance strategy to ensure cost-effective power generation while minimising life cycle expenses. Several studies have then been conducted where pattern recognition is carried out using techniques such as supervised learning classifiers, Wigner-Ville distribution, and filtered signal by Hilbert Transform [61, 62]. The approach taken by Arcos *et al.* filters the data set by wavelet transform, and the dimension of the signal is reduced by feature extraction and selection, followed by pattern recognition with supervised learning classifiers [63]. To note that although good results have been achieved, the cost and time-consuming process to acquire the necessary data for model training need to be taken into consideration when employing this method. Table 2.2 presents a summary of the techniques employed in plate-like structures [64].

Author	Year	Technique	Summary and results
Da Y. [42]	2017	Wavelet transform in time and wavenumber domains	Wavenumber-domain WT operation gives a better denoising effect than direct time-domain WT denoising. Using the former, one can perform the inverse flaw reconstruction by reflected signals with a SNR as high as -5 dB.
Xu C. [64]	2018	Dispersion compensation method based on compressed sensing	The method can compensate both single mode and multi-mode dispersive guided waves effectively, based on the accurate dispersion curves and every dispersive wave packet to the waveform of the excitation as well, and achieve better performance than the time-distance mapping method.
Wu J. [19]	2017	Smoothed Pseudo Wigner-Ville distribution and Vold-Kalman filter order tracking	The results of the simulation signal and the experimental signal reveal that the presented algorithm succeeds in decomposing the multi-component signal into mono components. Further research needs to be done to validate the feasibility of locating defects by the algorithm.
Chen Q. [45]	2021	ESPRIT and POS algorithms	The root mean squared errors between the estimated and theoretical dispersion curves calculated by the inversed model parameters for simulation, steel, aluminum and composite experiments are: 0.027, 0.032, 0.033 and 0.102 rad/m.
Sabeti S. [46]	2020	Spatio-temporal sparse wavenumber analysis	The results indicate the possibility of accurate reconstruction (correlation coefficient of around 0.9) for sampling rates above 60% of the spatio-temporal Nyquist critical sampling rate.

TABLE 2.2: Works found addressing signal processing techniques applied to plate-like structures.

Author	Year	Technique	Summary and results
Rizvi S. [48]	2021	Autoregressive model to modify the discrete Wigner-Ville distribution	The proposed method precisely estimated the distance between two closely spaced notches in a metallic plate from different simulated noisy signals with a maximum uncertainty of 5%.
Bagheri A. [49]	2016	Artificial neural network	The non-contact inspection system and the signal processing technique enable the classification of the plate health with a success rate ¿ 75 %.
Wang G. [51]	2019	Matching pursuit algorithm of Gabor function	The first iterative compensation of the proposed method can achieve compensation within the temperature range greater than 7°C, and the compensation within the temperature range greater than 18∘C can be achieved after three iterations.
Jia H. [50]	2020	Baseline-free method based on the mode conversion and the reciprocity principle	In the case of 1.0 mm depth, which performed strong ability of mode conversion, four obvious wave packets were observed. The result shows that the method could accurately localise both defects.
Douglass A. [52]	2018	Temperature compensation method based on dynamic time warping	For frequencies above 200 kHz and temperature differences above 25°C, the correlation coefficients were consistently greater than 0.75 while the scale transform showed correlation coefficients below 0.35. Correlation coefficients are consistent above 0.75 while the scale transform's correlation coefficient dropped to 0.45 with as little as 0.4 ms of data.

TABLE 2.2: continued.

Author	Year	Technique	Summary and results
He J. [54]	2019	Reverse-time migration (RTM) imaging	The algorithm was combined with a numerical simulator: the three-dimensional elastodynamic finite integration technique (EFIT), in order to provide multi-mode damage imaging. The results represent the damage location and size, but do not provide detailed information of different modes.
Lee Y. [56]	2021	Reconstruction algorithm for probabilistic inspection of damage (RAPID)	Location possibility was confirmed through the application of the anti-symmetric mode, and that quantitative imaging was very difficult in the bending stress dominant mode. The more accurate quantitative visualisation of defects was achieved when imaging was performed through this mode.
Xu C. [57]	2019	Weighted sparse reconstruction-based anomaly imaging method	Results for carbon fiber-reinforced polymer (CFRP) plate with an additional mass show that the weights constructed from the correlation coefficients between the scattering signal and the atoms of the dictionary are appropriate and accurate.
Zhang H. [58]	2018	Reverse time migration method	Numerical results demonstrate that the preprocessing of mode separation helps to effectively remove the artefacts resulting from the multi-mode interference in the process.
Lugovtsova Y. [60]	2021	Wavenumber mapping	The approaches used deliver an accurate estimate of the in-plane size of the large delamination at the interface, but only a rough estimate of its depth. The wavenumber mapping techniques used can quantify every delamination between CFRP plies caused by the impact, which is the case for conventional UT.

TABLE 2.2: continued.

Author	Year	Technique	Summary and results
Arcos Jiménez A. [63]	2019	Wavelet transform and supervised learning classifiers	Results show that the combination of the k-nearest neighbours algorithm with the principal component analysis technique provides the best results for the detection and diagnosis of mud in the developed experiments. The classifier that detects and identifies mud in all cases is the ensemble subspace discriminant model for E-1. Fuzzy k-nearest neighbours is the best classifier for E-2.
Tiwari K. [61]	2018	Wavelet transform	The discrete wavelet transform along with amplitude detection technique was applied on experimental B-scans to locate and size the defects with a significant accuracy: the percentage error was less than 12%.
Gómez Muñoz C. [62]	2018	Wavelet transforms	The envelope of the filtered signal by wavelet transforms is done based on Hilbert Transform, and the pattern recognition is achieved by autocorrelations of the Hilbert transform. The approach detects the ISO 12494 cases of un-frozen, frozen without ice, and frozen with ice in wind turbines.
Tiwari K. [65]	2017	Wavelet transform, Hilbert-Huang transform	The size of defects having diameters of 15 and 25 mm at -3 dB threshold level were measured as 9 mm with a percentage error of 40%, and 34.5 mm with a percentage error of 38%. The location of defects at the -3 dB threshold level from the start point of scanning was also calculated as 29 mm (for the defect of 15 mm), with a percentage error of 37.5%, and 405.5 mm (for the defect of 25 mm) with an error of 2%.

TABLE 2.2: continued.

2.2.3 Other geometries

Even though this review focuses on pipes and plate-like structures, it is important to point out certain methods that have been developed to adapt to other elements and geometries far more complex and thus, presenting a new set of challenges. For example, seven-wire strands when considered individually, resemble a hollow cylinder, but altogether the structure becomes complex and presents new complications.

In steel strands, He *et al.* utilised the lowest Longitudinal mode L(0, 1) as the excitation mode so that the received signal could be denoised with multi-level discrete wavelet decomposition and single branch reconstruction method [66]. Multi-level discrete wavelet decomposition is based on wavelet analysis, which produces a group of organised decompositions. By iterating the decomposition process, a signal is broken down into many lower-resolution components. To perform dispersion compensation, Legg *et al.* utilised dispersion curve data to characterise the wave propagation using broadband Maximum Length Sequence (MLS) excitation signal and spectrograms in overhead transmission cables [67]. Only the first set of echoes could be resolved without dispersion compensation, whereas with dispersion compensation and some filtering, individual echoes could be recognised for at least five sets of echoes from the end of the cable. While the study used an ACSR cable, the method can be applied to increase the inspection range for other structures, such as plates, pipes, and other types of cables. Ji *et al.* later applied singular value decomposition and support vector regression model to evaluate the stress level in strands, employing the theoretical and finite element methods to solve the dispersion curves of single wire and steel strands under various boundary conditions [68]. Despite simulated and experimental results showing the effectiveness and potential of the proposed technique, it is not always the best for visualisation. On the other hand, reliability can be enhanced by adding more samples.

Due to the intricate nature of these structures, machine learning techniques have been applied to further the interpretation of the signals. For example, by using a deep convolutional neural network (DCNN) with a VGG-like architecture-based regression model for detecting and estimating the looseness in bolted joints using a laser ultrasonic technique [69]. First, the signals are measured at each impinging point and then performed the imaging process to produce full-field ultrasonic data sets. These sets are then submitted to signal processing techniques and a model evaluation process is utilised for choosing the best performance. At last, the DCNN model is generated to estimate the looseness value of bolted joints. The ultrasonic receiver needs to be set up manually and can be applied in the straight-line area only. For beams, Liew C. introduced a multi-layer perceptron for pattern recognition, operating with one hidden layer of neurons and progressively trained using a backpropagation algorithm with integration of a weight-range selection (WRS) technique that was dependent on the test pattern to achieve good results for damage location and depth [70].

Importance is also placed on methods that can monitor practical structures with arbitrary complexity. Recently, Ju *et al.* proposed a new nonlinear guided wave technique to non-destructively determine the presence of microstructural defects in a large-area structure with complex geometry. When the multi-mode guided waves diffusely propagate through any physically-connected structure with arbitrarily complex geometry all available guided wave modes in any interrogated zone of the structure are automatically down-selected by the medium through attenuation, dispersion, or filtering. Such remaining modes efficiently transfer energy, for example, to their second harmonic modes, when they encounter micro-cracks even in the case of irregular geometries [71]. A summary of the techniques employed in these different structures can be found in Table 2.3.

Author	**Year**	**Technique**	**Summary and results**
He C. [66]	2008	Multi-level discrete wavelet decomposition and single branch reconstruction	The Daubechies wavelet of order 40 is used as the mother wavelet for the decomposition. This wavelet denoise method improves the SNR.
Legg M. [67]	2015	Dispersion curve compensation	Attenuation and dispersion compensation were then performed for a broadband Maximum Length Sequence (MLS) excitation signal. It was found that an increase in terms of SNR between 4 and 8 dB was observed relatively to the dispersed signal. The main benefit was the increased ability to resolve the individual echoes from closely spaced structures.

TABLE 2.3: Works found addressing signal processing techniques applied to other structures.

Author	Year	Technique	Summary and results
Ji Q. [68]	2021	Singular value decomposition and support vector regression	Results show that the fundamental mode dispersion curve offset on the high-frequency part and cut-off frequency increases as the boundary constraints enhance, demonstrating the capability of the proposed support vector regression method for evaluating the stress level in the strands.
Tran D. [69]	2020	Discrete convolutional neural network	The DCNN and wave propagation imaging produced the highest R2 score and lowest MSE score: 0.91 and 1.55, respectively.
Liew C. [70]	2008	Series combined network with the integration of a weight-range selection	The system was able to achieve average predictions accurate to 2.5 and 7.8% of the original training range sizes for the damage location and depth, while the WRS provided up to 13.9% improvement compared to equivalent conventional neural networks.
Ju. T. [71]	2022	Nonlinear response of multi-mode guided wave ultrasonic signals	Experimental results are consistent with numerical simulations, indicating that the proposed method can be implemented for semi-quantitative detection or early warning indication of microstructural defects in complex, large-area structures.

TABLE 2.3: continued.

2.3 Summary

Ultrasonic guided wave testing is a dominant field in structural health monitoring and non-destructive testing, serving as an effective long-range inspection method. Nonetheless, the multi-modal and dispersive nature of guided waves makes signal processing a particularly difficult task. This review aimed at presenting an overview of signal processing techniques applied to guided waves. Numerical methods to improve the SNR, isolate and separate modes, and identify and classify defects were discussed in terms of effectiveness and limitations, along with machine learning techniques that can be integrated, which is an approach that shows promising results in the field. New lines of research can be brought to light with the understanding of the aforementioned issues in terms of ultrasonic guided waves. The solution seeks to improve the capacity of UGWT to detect damage in all sorts of structures in a more informed and reliable manner.

Chapter 3

Split Spectrum Processing

3.1 Introduction

As previously stated, one of the most common issues signal processing techniques applied to UGWT aim to solve is to eliminate dispersive modes, thus increasing the spatial resolution and enabling the detection of defects. Several methods can be employed to this end, but the following section describes a specific technique that is commonly used, due to its simplicity and low computational cost. This method has been widely studied and has a long history in the field of NDT to reduce grain scatter. To reduce the effect of dispersion, a few things can be done in terms of pre-processing, such as utilising short pulses and axisymmetric wave modes for excitation. However, the interaction between the signal and features found along the structure will result in mode conversion and thus give rise to dispersive modes. These modes spread out in time and space, making signal analysis and identification of certain defects a complex task. Another issue that emerges is the fact that dispersion is one of the main sources of coherent noise, meaning noise that is non-random and occupies the same bandwidth as the target signal. Therefore, conventional filtering techniques such as low pass and high filters are ineffective in filtering the signal. It is also important to note that these modes can contain relevant information regarding defects present in the structure, so their removal is not ideal. However, mode separation is quite difficult to achieve.

Dispersive modes are characterised by their frequency-dependent properties, such as their group and phase velocity and when graphically represented are often referred to as dispersion curves (Figure 3.1). The presence of these modes leads to overlaps of the signal in the time domain and group delays. In pipes, the modes supported are Longitudinal

L(0,m), Torsional *T(0,m)* and Flexural *F(n,m)*, where n is the circumferential order and m corresponds to the mode order. Torsional and Longitudinal modes are axisymmetric and thus their circumferential order is 0. Flexural modes contrastingly can have three different configurations in terms of circumferential order (Figure 3.2).

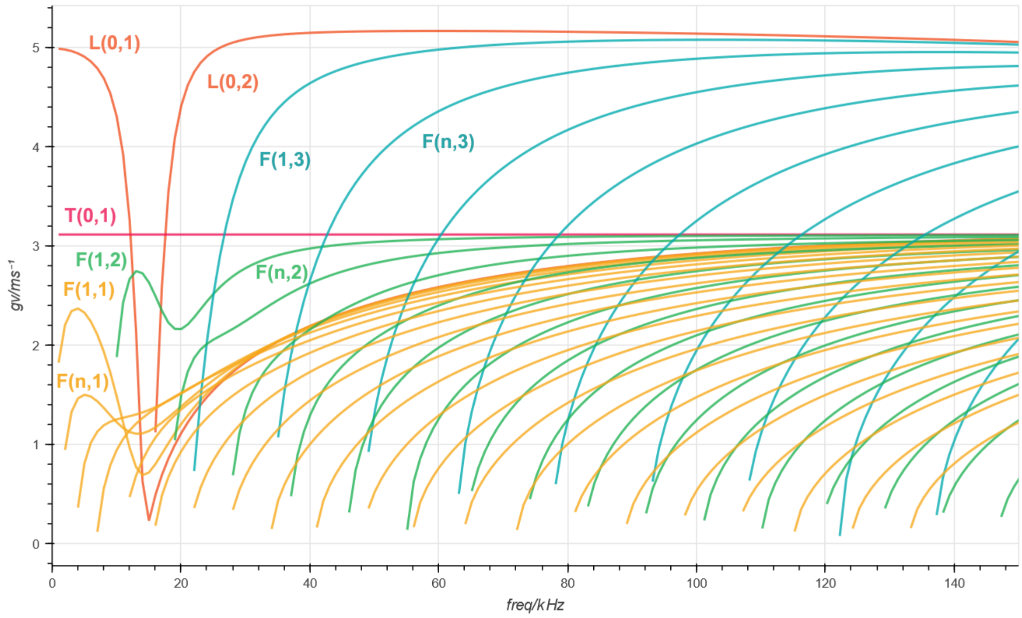

FIGURE 3.1: Group velocity dispersion curves for a 4 inches carbon steel pipe. The order n of the flexural modes increases from left to right.

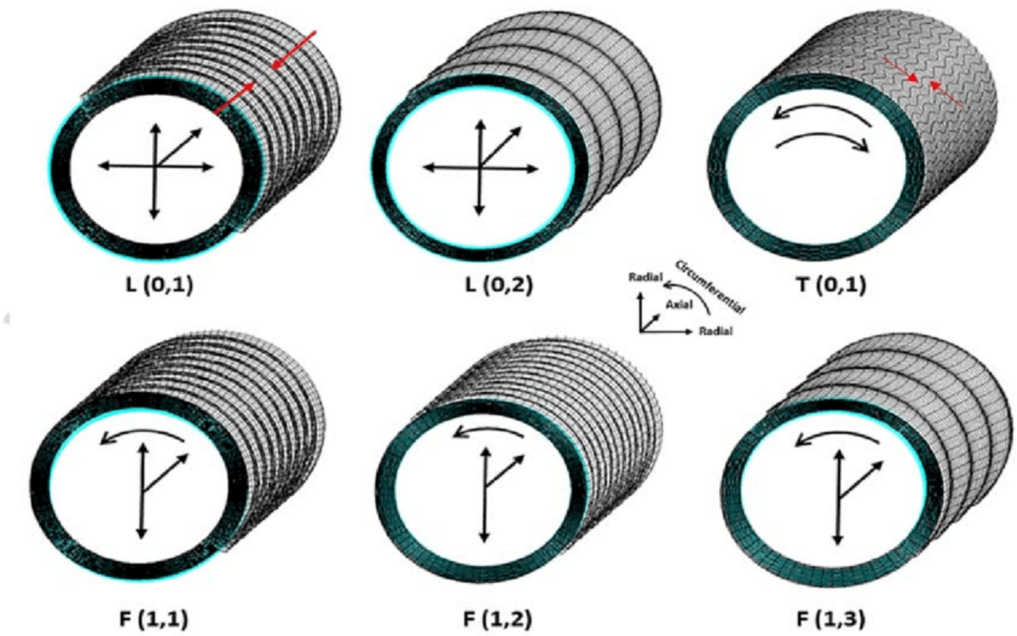

FIGURE 3.2: Selection of displacement shapes of guided wave modes in a 6-inch steel pipe at 60 kHz [72].

Split spectrum processing is a signal processing method that aims to increase the SNR of a given input signal by reducing the coherent noise. It is worth noting that, as stated above, it is not suppressed during the averaging and cannot eliminate by using conventional filtering algorithms because it is at the same frequency band as the signal of interest. It was first applied in radar applications having later been adapted to ultrasonic guided wave testing. The method consists of splitting the input signal into various sub-bands using a generated bank of band-pass filters followed by the recombination of those same sub-bands. The input signal $x(t)$ is converted from time-domain to frequency domain using the Fourier transform, thus obtaining the signal $X(f)$. A filter bank is then utilised to split the signal into bands. To create the filter bank, it is necessary to select the bandwidth of interest, which is then split into equally spaced band-pass filters at different centre frequencies obtaining insights into the spatial distribution of energy in each band, resulting in a number of output signals $X_n(f)$ $(n = 1, 2, ..., N)$ where N is the total number of filters. These signals are then converted back to the time domain using inverse FFTs and normalised by a weighting factor where each set of signals is divided by its maximum values in the time domain before the recombination algorithms are applied. Finally, they are recombined through non-linear processing procedures to identify the areas of the signal in which there is a significant contribution of energy present in all bands, such as averaging, minimization and order statistic filters that differentiate target echoes from clutter. (Figure 3.3).

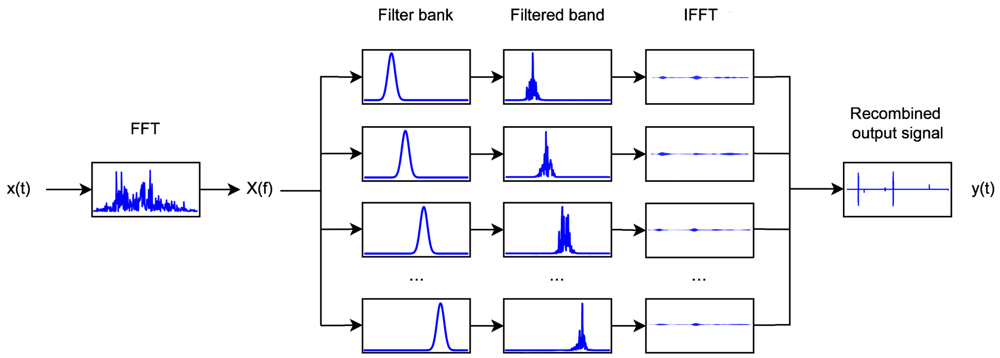

FIGURE 3.3: Schematic diagram of the split spectrum processing technique.

The velocity of the different modes can be represented using dispersion curves as a function of frequency. Dispersion experienced by the wavefront is dependent on frequency, depending on the size, number and distribution of the scatterers of the material, thus for dispersive modes, not all the frequencies will be reflected equally, a phenomenon called frequency diversity. Thereby, the presence of dispersive modes across the sub-bands will vary as opposed to non-dispersive modes, which will stay constant. Split spectrum processing explores the frequency diversity phenomenon. By filtering these sub-bands, the algorithm removes the components that differ along the bandwidth. The spectral power density of the received echo will only carry information on a few localised bands when the wavefront collides with a reflector of size proportional to its wavelength. The size and distribution of these reflectors are random, and so is the distribution of the received power.

3.2 Selection of bank filter parameters

Following the conversion from time-domain to frequency-domain using the FFT, it is necessary to divide the signal into the desired sub-bands. Thus, a bank filter must be designed to achieve this end.

The parameter values of the filter bank were first studied by means of trial-and-error for NDT applications as they were processed. This approach is, however, not practical since inspection requires large sets of data to be constantly analysed. In conventional ultrasonic applications, the SSP algorithm has been successfully employed due to ideal parameter selection. Nonetheless, the parameter selection rules used for SSP of conventional UT signals are unsuitable for signals used in UGWT due to the comparatively long duration and narrow bandwidth. These signals also contain axisymmetric and non-axisymmetric wave modes with different phase velocities. So, the proper selection of optimum filter bank parameters is required to obtain adequate results.

Several factors contribute to this task, such as the number of bands N, the total operating bandwidth for processing B and the bandwidth of each filter B_{filt}, the overlap between the bands, and the filter separation F and the filter type. The design of the bank filter itself depends on the following parameters:

- **Total operating bandwidth B**: corresponds to the bandwidth in which the signals from features are constant across its range, and the coherent noise varies. If the bandwidth is too wide or too narrow, then at least one of the filter outputs will not include the feature signal, and this may cause the feature to be lost in the process.

- **Filter separation F**: the filter separation is the distance between sub-band filters based on the parameter selection in SSP for conventional UT. According to the literature, the optimum spectral splitting could be achieved using the frequency-sampling theorem. The frequency-sampling theorem says that the spectrum of a time-limited signal can be reconstructed from its sample points in the frequency domain.

- **Sub-band filter bandwidth B_{filt}**: corresponds to the width of each filter used in the filter bank. Since the bandpass filter can reduce the temporal resolution of the signal because reducing the bandwidth of a time-limited signal will increase its duration, applying the SSP filter banks could lead to a reduction in temporal resolution if not suitable, as the pulses that correspond to reflections from features spread out in time and masks one another.

In conventional UT, the transmitted signal is usually an impulse function and, therefore, the bandwidth is limited by the frequency response of the transducers. As a result, the processing bandwidth in conventional UT is often the frequency response of the ultrasonic transducers. These parameters are not independent, as changing one value will require the other values to change. For instance, increasing the filter bandwidth would signify a reduction in the number of filters or the value for filter separation.

The filter bank parameters must be chosen carefully since the method is highly sensitive to the values selected. It also depends on how well the observations and statistical data in each channel correlate.

The ideal values do not follow a linear trend, as was previously mentioned, and changing one value automatically changes the others. For example, while increasing the number of channels of band-pass filters increases the likelihood of detecting target echoes against the undesirable microstructure scattering noise, there is only a limited number of information-bearing frequency bands. So, increasing the number of channels may result in many observations that only contribute to clutter echo information. In contrast, if the channel bandwidth is too small, flaw echo information is concealed because of resolution loss. Disproportionate frequency overlap between channels, on the other hand, results in excessive correlation among the channels and limits the anticipated TCR improvement.

It is also found that for a large overlapping of bands, the signals are highly correlated, and SNR is not improved, whereas narrow filters result in the loss of relevant information to defect detection. Thus, the overlap chosen should minimise the correlation between

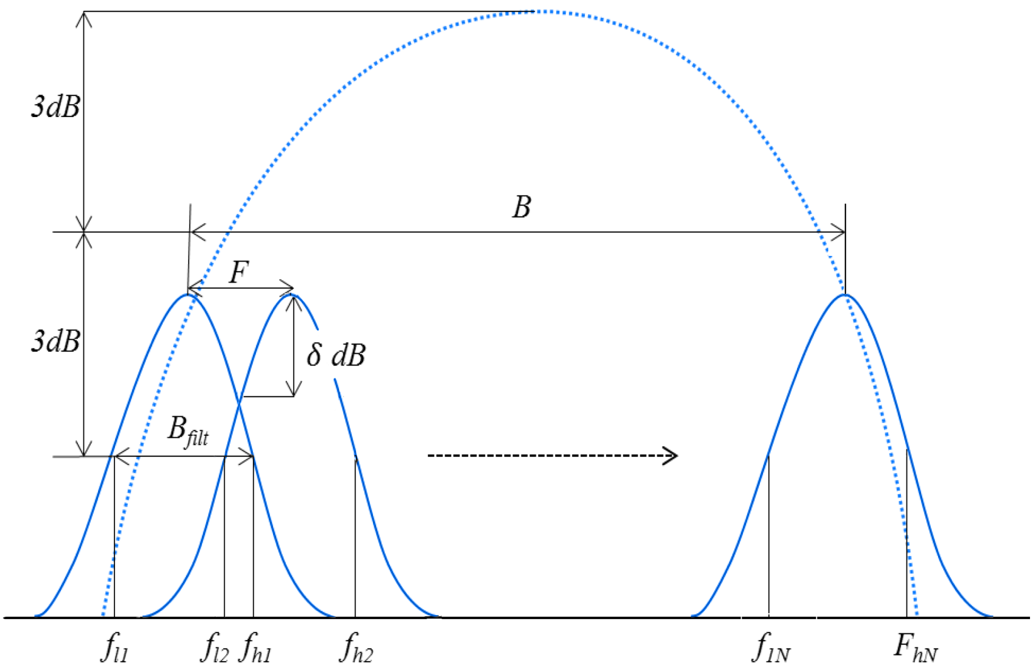

FIGURE 3.4: Frequency band-pass filter bank parameters for SSP using the gaussian window function. B is the total bandwidth, F the filter separation and B_{filt} the sub-band filter bandwidth.

noise regions in adjacent sub-bands without losing information. To obtain an accurate target detection it is ideal to develop a technique that offers minimal sensitivity to the filter frequency coverage.

All these trade-offs need to be therefore considered when making the selection of the bank filter parameters in practical use.

3.3 Recombination algorithms

Once each signal has been filtered and split into different frequency bands, all the resulting signals must be recombined to determine which part of the original signal stems from a defect. For this end, several algorithms can be employed. Methods such as minimisation, median and maximisation are referred to as order statistical methods, in which sample values are arranged in ascending order. The use of these ordered variables and their functions are the focus of the study of order statistics, and it can also be used to describe statistics that do not depend on the values themselves, but rather simply on their ordering. Order statistics concepts have achieved successful results when applied to conventional ultrasonic testing applications such as radar, sonar and image processing. If we added the sub-bands linearly, the original SNR would be restored. Because these methods are non-linear, it's expected that the amplitude of a feature will increase, and the noise will be reduced. The most common techniques used in the literature are described in more detail below.

3.3.1 Minimisation

The output $y[m]$ of each instance of time is the minimum of the absolute value of all sub-bands:

$$y_{MIN}[m] = min(|x_1[m]|, ..., |x_n[m]|) \tag{3.1}$$

The minimisation algorithm reduces the noise as it varies across each sub-band. Since the variation of noise is expected to be greater than the signal variance, this technique is most effective when the noise level is low in comparison to the signal and when the target echo information exists in all frequency bands. This method offers very little resolution and often high SNR values cannot be reached.

3.3.2 Polarity threshold

Polarity threshold takes on the value of the input signal if all sub-band time samples $x_i[m]$ are either positive or negative, otherwise the signal is zero:

$$y_{PT}[m] = \begin{cases} x[m], & \text{if all} \quad x_i[m] > 0 \\ x[m], & \text{if all} \quad x_i[m] < 0 \\ 0, & otherwise \end{cases} \tag{3.2}$$

In this method, only the time samples where the polarity remains unchanged pass, making it so that only time samples not affected by frequency are considered. As a downside, it requires a large number of sub-bands to achieve a significant gain in SNR.

3.3.3 Polarity threshold with minimisation

To further suppress noise effect, polarity threshold with minimisation combines the previous two methods by looking at the sub-bands in each sample time and if the samples are all positive or all negative then the signal takes on the minimum value found in the sub-bands, otherwise, the output is zero:

$$y_{PTM}[m] = \begin{cases} min(x_i[m]), & \text{if all} \quad x_i[m] > 0 \\ min(x_i[m]), & \text{if all} \quad x_i[m] < 0 \\ 0, & otherwise \end{cases} \tag{3.3}$$

This has the effect of only passing time samples where polarity is not affected by frequency. Therefore, those parts of the signal that are highly frequency-dependent should be removed. Reducing the noise level will considerably lower the signal amplitude in some sub-bands and provide the lowest values for the PTM's output, as this technique loses effectiveness when the noise level exceeds the actual signal.

3.3.4 Scaled polarity threshold

Also called polarity threshold with probability scaling, by scaling the polarity threshold algorithm it is possible to obtain a different recombination algorithm, in which the minimum amplitude is multiplied by a function of the number of filtered signals with the same sign:

$$y_{SPT}[m] = \left(\frac{p_+ - p_-}{n}\right)^{n/2} \times min(|x_1[m]|, |x_2[m]|, ..., |x_n[m]|) \times 4n \tag{3.4}$$

The approach based on phase deviation is similar to the polarity threshold with scaling, in which the phase refers to the polarity of the filtered signals.

3.3.5 Mean algorithm

The output of the mean algorithm, y_{mean} is the summation of the mean of each of the N sub-bands sample at that sample time:

$$y_{mean}[m] = \frac{1}{N}\sum_{i=1}^{N} x_i[m] \tag{3.5}$$

This algorithm is more suitable for a signal with low levels of noise since the amplitude decreases when the noise level is high.

3.3.6 Normalisation

The normalisation technique takes the minimum of the absolute value from all bands, previously normalised by the greatest value of each of them $\hat{x}_i[m]$, for each moment in time (distance):

$$\hat{x}_i[m] = \frac{x_i[m]}{max(x_i[m])} \tag{3.6}$$

$$y_{NORM}[m] = min(|\hat{x}_1[m]|, |\hat{x}_2[m]|, ..., |\hat{x}_n[m]|) \tag{3.7}$$

This algorithm divides each channel output energy by their maximum, in order to obtain true sensitivity to only each channel's varying tuning frequencies, making this measurement independent of the absolute magnitudes.

3.3.7 Frequency multiplication

This technique is relatively similar to the mean algorithm, taking the product of the time samples from all bands:

$$y_{FM}[m] = x_1[m] \times x_2[m] \times ... \times x_n[m] \tag{3.8}$$

It provides good resolution and good results for SNR improvement when combined with variable bandwidth filters, equally spaced and energy equalised, requiring fewer sub-bands when the material has low dispersion. However, for a bank filter with constant bandwidths, the result worsens.

3.4 Algorithm evaluation

The evaluations of each recombination algorithm and filter bank in terms of defect detection can be calculated through the signal-to-noise ratio, measured in dB:

$$SNR = 20 \log \left(\frac{S}{N} \right) \tag{3.9}$$

where S is the amplitude of the target signal and N the amplitude of the average noise present in the location of the target signal. The improvement of the SNR can be determined in regard to the SNR of the original signal and the SNR of the resulting filtered output after the application of the different recombination algorithms:

$$SNR_{enhanced} = SNR_{output} - SNR_{input} \tag{3.10}$$

The resulting output should also be able to identify the position of the defects present in the structure, as well as eliminate dispersive modes. The SNR improvement of each algorithm with the suggested bank filter can then be compared to determine the best fit for the processed signals.

3.5 Algorithm Implementation

In this section, each step of the implementation of the SSP algorithm is explained in more detail. The program was written in Python, and it takes an input signal. An MOT (Magnetic Optical Transducer) is an ultrasonic-based screening technique that emits the initial impulse signal that propagates along the pipeline and the signal is received by a Michelson Interferometer with fibre lengths of 1.5 m. These signals are then processed and analysed. The algorithm generates the sub-bands and then employs the various SSP recombination algorithms mentioned in section 3.3.

3.5.1 Pre-processing filtering of the input signal

The input signals studied contain some form of noise that can be filtered through conventional methods. To accomplish this, the first step in the pre-processing stage consists of filtering the signal using a Butterworth filter. A Butterworth filter is a processing filter designed to have a frequency response that is as flat as possible in the passband. The filter used is of second order, which decreases at -12 dB per octave. Figures 3.5 and 3.6 represent the original input signal and the filtered signal respectively. For the implementation of this filter, the function used comes from a library authored by EQS.

The distance travelled by the signal can be obtained by dividing the time it takes to reach the sensor by the average velocity of the signal. In this specific case, it corresponds to a value of around 3420 ms^{-1}. It's important to point out that external factors such as temperature and mode conversion inside the pipe lead to variations in the signal velocity, which consequently may lead to eventual deviations from the accurate value. The velocity variation will, in the end, affect the results for the position of a detected defect that can be translated to a few centimetres. In the context of the inspection industry, this deviation does not present much significance as a deviation in the order of meters.

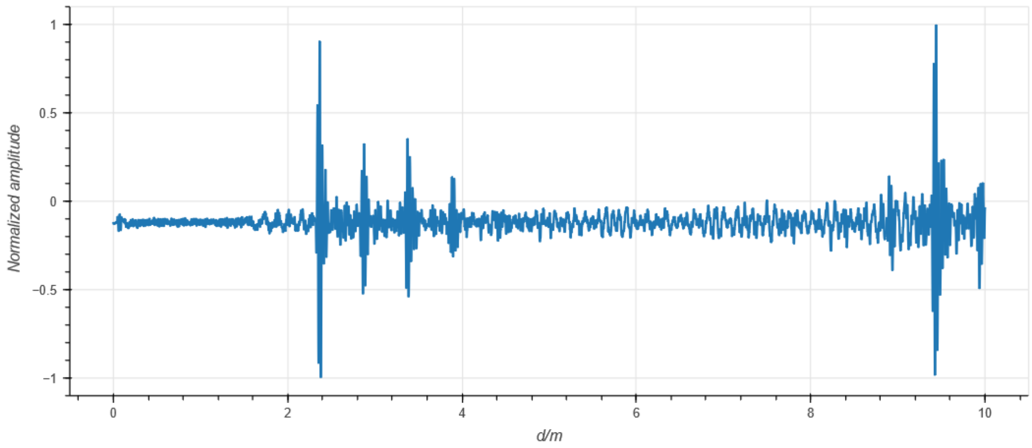

FIGURE 3.5: Ultrasonic guided wave input signal measured with a Michelson interferometer with a frequency of 70 Hz.

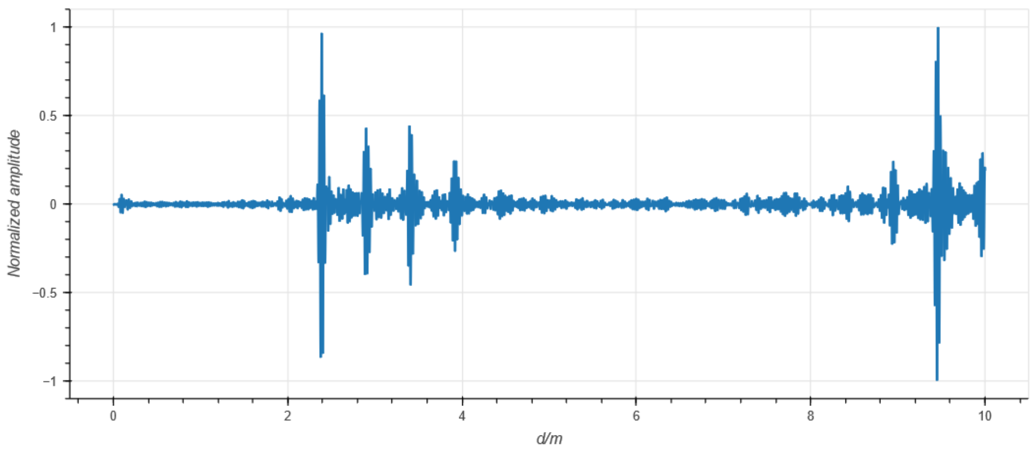

FIGURE 3.6: Filtered result signal with a second order Butterworth filter obtained from the signal shown in Figure 3.5 for a length of 10 meters.

As it is possible to confirm in the graphs represented above (Figures 3.5 and 3.6), the filtered signal presents a signal with a lower noise level, but the dispersive modes are still present. This is due to reasons stated before, since the coherent noise occupied the same bandwidth as the emission signal it is impossible to eliminate them through traditional filtering techniques.

3.5.2 Fast Fourier Transform

The program then converts the signal from the time domain to the frequency domain using the Fast Fourier Transform. The Fast Fourier Transform computes the discrete Fourier transform of a signal and the frequency domain is obtained by decomposing a sequence of values into components of different frequencies. It is often used in applications such as digital recording, sampling, additive synthesis and pitch correction software. The significance of the FFT stems from the fact that it has made frequency domain work computationally as possible as temporal or spatial domain work. It can be defined as:

$$X(m) = \sum_{n=0}^{N-1} x(n) e^{\frac{-j2\pi mn}{N}} \tag{3.11}$$

The graphical representations of the FFT for both the original input signal and the filtered signal correspond to the graphs below (Figures 3.5 and 3.6). The amplitudes have been normalised to make their interpretation easier.

As expected, the input signal contains a range of frequencies around 10 kHz and 20 kHz that comprises noise derived from vibrations and other non-systematic sources of error. The Butterworth filter takes the input signal and its sampling frequency and can eliminate non-coherent noise. Coherent noise, however, as is the case for undesired dispersive modes, exists in the same bandwidth as the signal. The designed filter bank has then to cover the whole bandwidth of the filtered signal to eliminate dispersive modes.

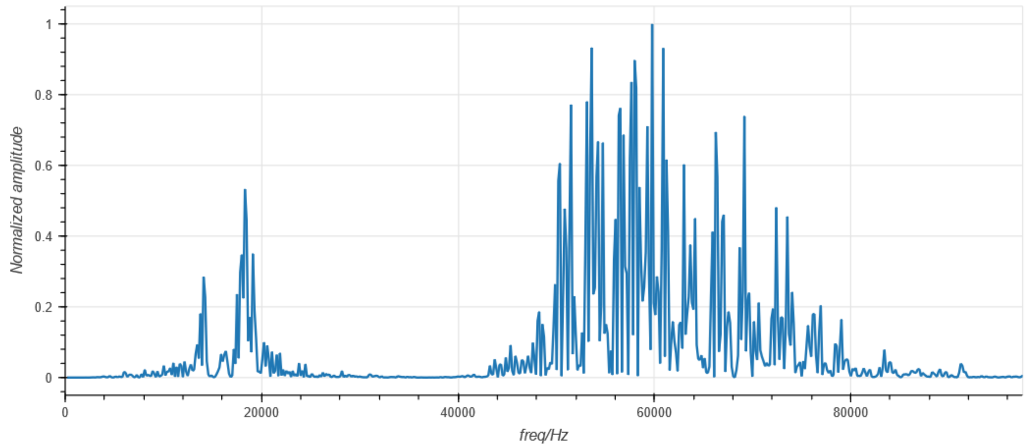

FIGURE 3.7: Fast Fourier transform of the input signal represented in figure 3.5.

The STFT (Short Time Fourier Transform) has also been represented for the input signal and the filtered signal, as done previously, in figures 3.9 and 3.10. This function allows the sinusoidal frequency and phase content of local sections of a signal to be determined as it changes over time. It is an important tool to verify the dispersive characteristic of the signals. The colour bar on the side of the graphs represents the magnitude of the power spectrum. The process for computing STFTs entails splitting a longer temporal signal into equal-length shorter segments before separately performing the Fourier transform

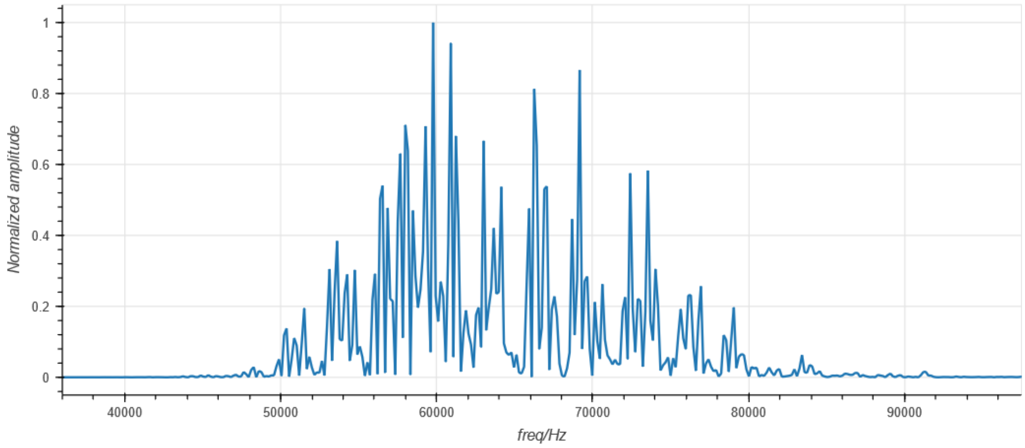

FIGURE 3.8: Fast Fourier transform of the input signal represented in figure 3.6.

on each of these shorter segments. In each shorter section, exposes the Fourier spectrum. The changing spectra are then typically plotted on a spectrogram, which is a function of time or distance. Besides the possibility of observing dispersive signals, its applications include the location of frequencies of specific noises (especially when used with greater frequency resolution) or to find frequencies which may be more or less resonant.

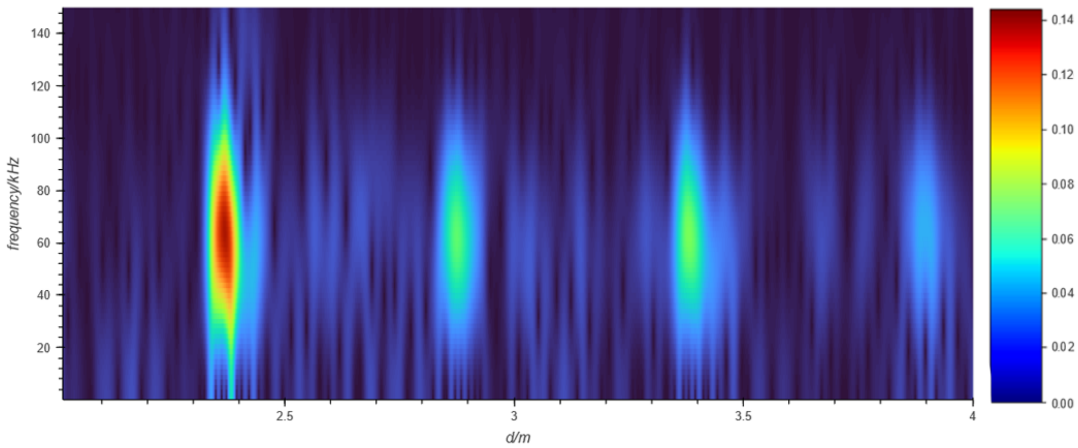

FIGURE 3.9: Short Time Fourier transform of the input signal represented in figure 3.5 between 2 and 4 m.

Having obtained the frequency spectrum, the next step is to move onto the division of said spectrum in the sub-bands, described in detail in the next section.

3.5.3 Filter bank design

The main component of the Split Spectrum Processing technique lies in the design of the filter bank that as the name indicates, splits the frequency spectrum of the input signal into sub-bands that are then combined to generate an output that filters dispersive modes.

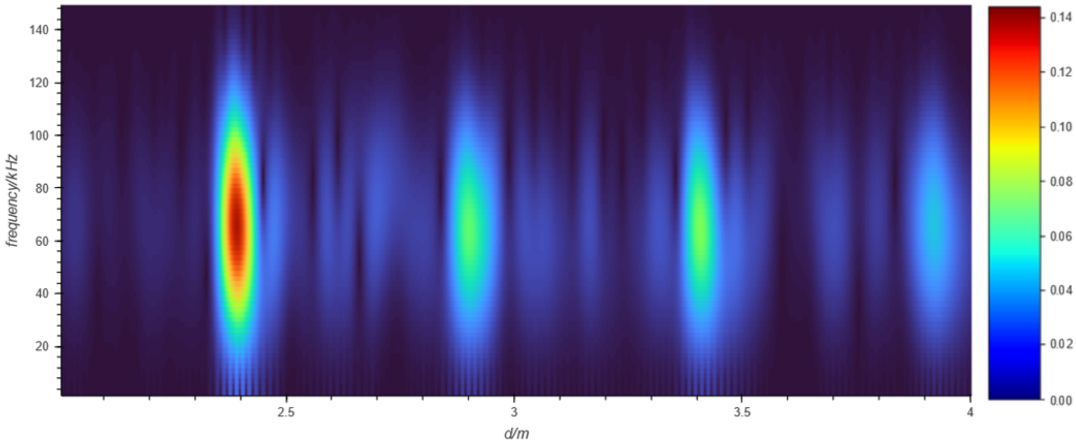

FIGURE 3.10: Short Time Fourier transform of the input signal represented in figure 3.6 between 2 and 4 *m*.

In earlier works, the implementation of the filter bank is based on the use of *sinc* functions in UT applications. However, in UGWT it's common to utilise the Gaussian filter instead, so some parameters obtain a greater value than expected. Most of the literature consulted makes use of the Gaussian window. The only specific justification for the choice of the Gaussian filter in any of the publications was its simplicity of implementation. The Gaussian window is employed with the following equation:

$$w(x) = \exp\left(-\frac{1}{2}\left(\frac{x - x_c}{\sigma}\right)\right)^2 \tag{3.12}$$

$$\sigma = \frac{FWHM}{2\sqrt{2\ln(2)}} \tag{3.13}$$

where x_c is the center, σ the standard deviation and FWHM corresponds to the full width at half maximum. The definition of these variables according to the filter bank are described below.

To design an adequate filter bank, it is necessary for it to cover the total operating bandwidth B, as it was explained in section 3.2. To generate the filter bank, a set of 3dB cut-off frequencies for the Gaussian filters are applied so that the lower and higher cut-off frequencies for each sub-band filters are calculated as:

$$f_{l_n} = \begin{cases} f_{min} - F, & n = 1 \\ f_{l_{n-1}} + F, & n = 2, 3, ...N \end{cases} \tag{3.14}$$

$$f_{h_n} = f_{l_n} + B_{filt}, \quad n = 1, 2, ...N \tag{3.15}$$

where f_{l_n} is the lower cut-off frequency and f_{h_n} is the higher cut-off frequency of filter n, N is the number of filters, F is the filter separation and B_{filt} is the sub-band filters. The value of the lower cut-off frequency for the first sub-band has to cover the start point of the signal, so it is defined as the difference between f_{min} and F.

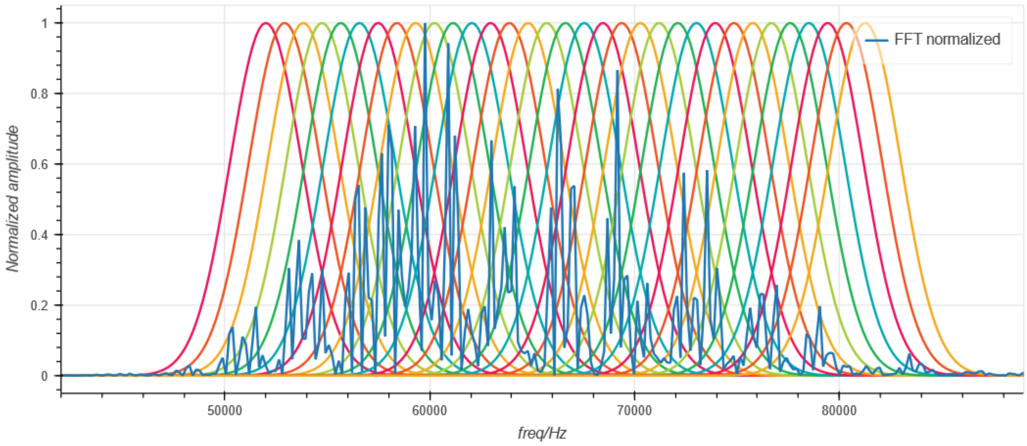

FIGURE 3.11: Normalised Fast Fourier transform overlap with a filter bank of Gaussian filter windows resulting from non-optimised parameters.

The selection of these values is based on the values often chosen for the implementation of the technique in conventional UT. So, these values need to be adjusted for UGWT. This can be achieved through a brute-force search algorithm. In computer science, a brute-force search algorithm or exhaustive search is a problem-solving technique that entails methodically listing every possibility for the answer and determining whether each one satisfies the problem's statement. In this case, the optimum parameters can be determined by choosing the set of parameters that eliminate dispersive modes and obtains the highest values for SNR enhancement whilst identifying the features and defects present in a pipeline.

The parameters required to implement the SSP technique are the total operating bandwidth for processing B, the filter separation F, the number of filters N, and the sub-band filter bandwidth B_{filt}. As stated previously, the variation in one of these parameters will change the values of the others. To reduce the effect of dispersive modes and suppress the dispersion effect in UGWT, narrowband waveforms are used in excitation signals. This makes it so that the bandwidth of the transmitted signal can be used for SSP while considering the frequency response of the transducers.

To determine the ideal SSP parameters for the signal in question, the SSP parameters were varied and applied, repeating the processing for all possible combinations to find the set of parameters that provided the best performance. The values used for conventional UT served as inspiration for the ranges of values used in the brute force search process, which corresponds to the following:

- B between 84% and 100% in steps of 3%.
- B_{filt} is B divided by values between 3 and 15 in steps of 2.
- F is defined as B_{filt} divided by 1.5 and 6.5 in steps of 1.

This results in 255 different combinations of parameter values. Because the signals studied propagate in the same pipe with known dispersion characteristics (in this case it was used a 4 inches carbon steel pipe in which the dispersion curves behaviour is represented in figure 3.1), the SSP parameters can be determined in controlled conditions. As mentioned before, the performance of each set is evaluated by measuring the SNR of the output signals. All combinations were represented for different signals and cross-referenced to obtain the optimum parameters. The best results were obtained when the parameters were set as follows:

- 90% of the total operation frequency.
- A sub-band filter bandwidth that is equal to the total operating bandwidth divided by 7.
- A filter separation that is equal to the sub-band filter bandwidth divided by 4.5.

These parameters were then applied to data acquired in different conditions for the approach to be validated. The analysis of the experimental data obtained detailed in the following section is done based on these parameters.

SSP parameters	**Optimum values**
Total bandwidth B	90% of total energy
Filter bandwidth B_{filt}	$B/7$
Filter separation	$B_{filt}/4.5$
Number of filters N	$(B/F)+1$

TABLE 3.1: Optimum paramenters for the design of the filter bank for split spectrum processing implementation.

Since pipes made of the same material, structure and cross-sectional geometry possess the same guided wave characteristics, then the relative rates of dispersion between the acceptable wave modes and the undesirable wave modes will be the same. From this, it's expected that if the ideal SSP parameters are determined for a pipe with specific characteristics, then these same parameters can be successfully applied to pipes with similar characteristics. This is quite useful in the industry since regulations make it so that manufactured pipelines are produced from a limited set of standards. Therefore, if the pipes are similar, it's not necessary to find the optimum parameters every time a pipe is inspected.

After the bank filter has been designed, the input signal can be filtered using each one of the Gaussian bandpass filters in the frequency domain and multiplying them by the Fourier transform. An example is illustrated in figure 3.12.

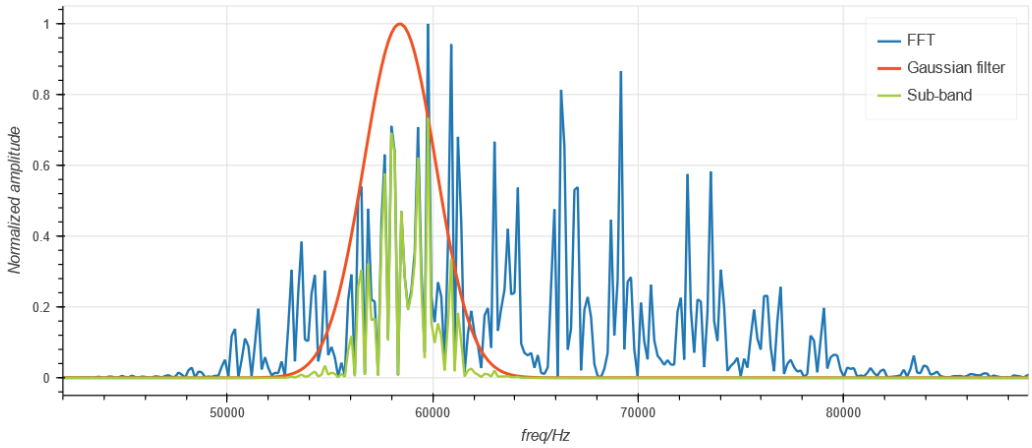

FIGURE 3.12: Normalised FFT overlaped with a gaussian filter. The window is multiplied by the FFT function, spliting the spectrum in a sub-band.

The selected sub-band is multiplied by the FFT function, thus splitting the spectrum, resulting in a signal that is equal to the FTT representation in a given range of frequencies and equal to zero otherwise. This process is repeated for all sub-bands present to obtain an assortment of sub-bands that cover the whole spectrum, represented in figure 3.13.

3.5.4 Inverse Fast Fourier Transform

Once the set of sub-bands has been obtained, each band needs to be converted back to the time-domain in order to be processed by the recombination algorithms. This can be done through the application of the inverse FFT:

$$x(n) = \frac{1}{N} \sum_{m=0}^{N-1} X(m) e^{\frac{j2\pi mn}{N}} \tag{3.16}$$

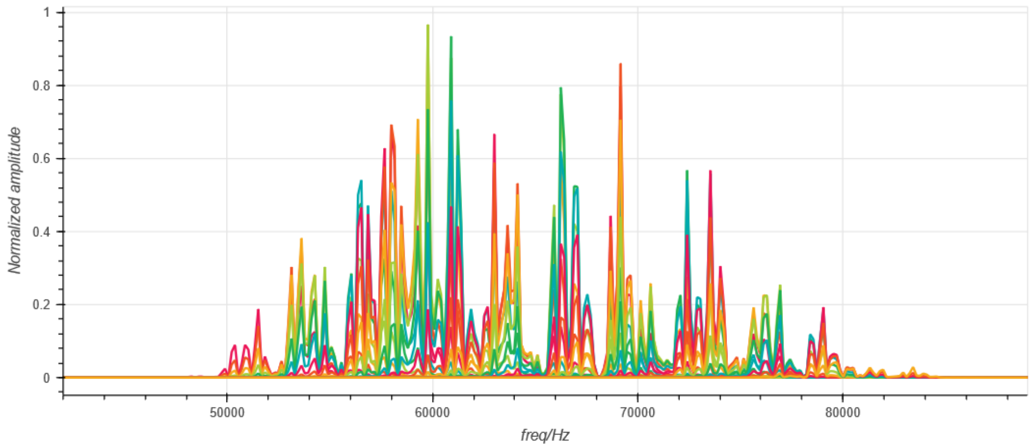

FIGURE 3.13: Representation of all sub-bands obtained from the splitting performed by the filter bank.

Each sub-band was first multiplied by the maximum of the signal's FFT to denormalise the functions. Following this step, all of the bands were individually converted from the frequency domain to the time domain. Each element is normalised by a weighting factor where each set of signals is divided by its maximum values in the time domain. The representation of all bands is present in figure 3.14. Once this process is done, the sub-bands can be recombined utilising different non-linear recombination algorithms mentioned in section 3.3, to obtain an output signal. This output should identify the locations of all frequencies to determine which portion of the signal presents a real defect.

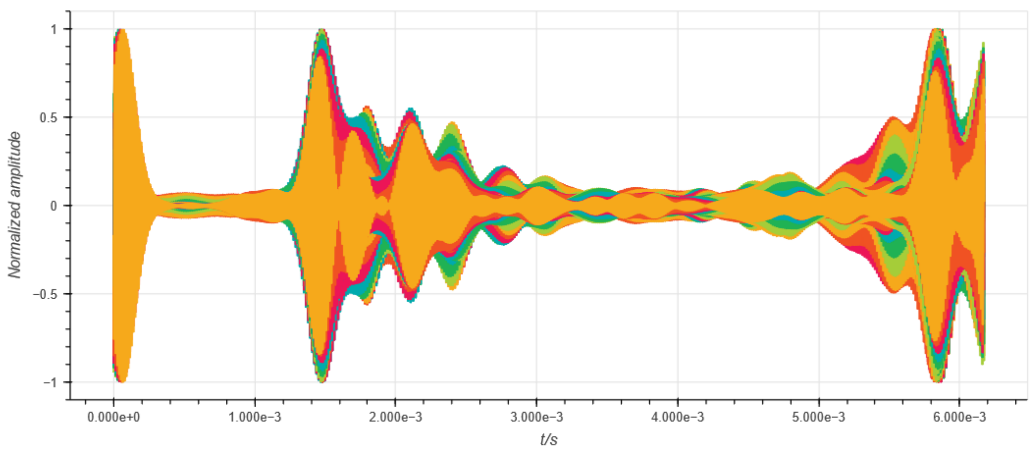

FIGURE 3.14: Inverse Fast Fourier transform of one of the sub-bands obtained from the spectrum splitting.

3.5.5 Recombined output signals

Having obtained the sub-bands in the time-domain, they can now be recombined using the algorithms detailed in section 3.3.

The program was written in Python and takes as the input the set of sub-bands obtained from each signal and recombines them non-linearly so that the location of the signal where the frequency remains unchanged can be detected. As shown in figure 3.15, the outputs of all the SSP recombination algorithms exhibit some significant improvement in terms of SNR values. The figure shows that the mean algorithm presents very little improvement. The best results are obtained for the polarity threshold and polarity threshold with minimisation. The FM algorithm minimises the pipe's end amplitude and removes the reflection signal from the defects. This distortion results from the multiplication of each sub-band's frequency without taking into account the signal's sign. The remaining algorithms provide some enhancement, but the spatial resolution of the result compared to polarity threshold and polarity threshold with minimisation algorithm are worse. The results indicate that the unprocessed signal has a lower likelihood of correctly identifying flaws since they are at a similar level to the background coherent noise created by the presence of dispersive wave modes. The proposed SSP method, including PT and PTM, on the other hand, eliminates the noise and just the defect's reflection is left, with no signal distortion. The improvement in SNR values is dependent on the level of input noise and level of dispersion so for a signal with low values of noise and dispersion, the algorithm's performance will increase.

The implementation of the SSP technique was achieved, along with the design of the filter bank and the selection of the parameters that maximise the SNR values of the signal. In the next chapter, the results obtained are applied to a structure with known features to accurately determine the precision and success of the algorithm.

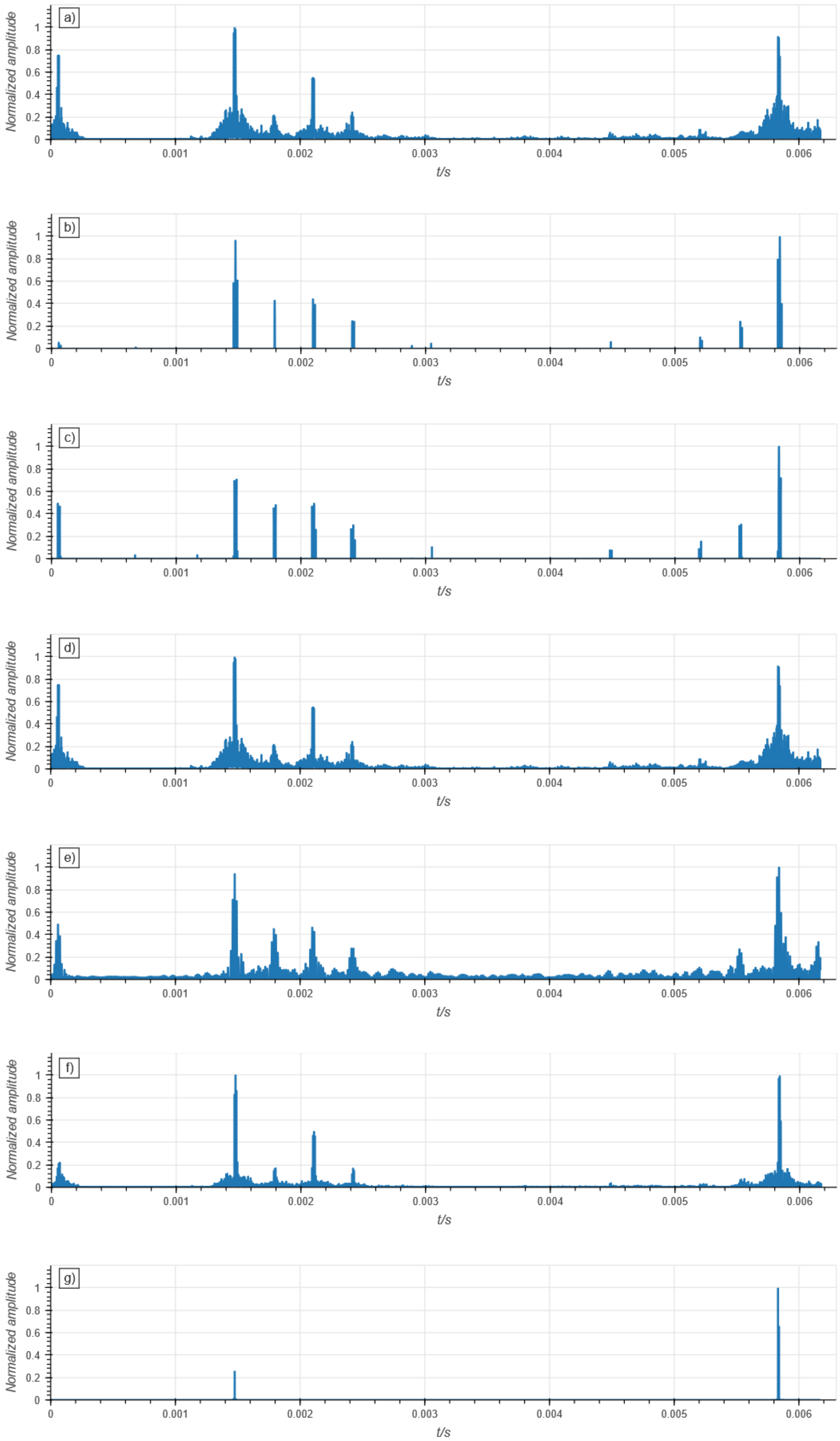

FIGURE 3.15: Results obtained for the a) minimisation, b) polarity threshold, c) polarity threshold with minimisation, d) scaled polarity threshold, e) mean, f) normalisation and g) frequency multiplication recombination algorithms.

Chapter 4

Results

4.1 Synthesization of dispersive signals

To first make sure the technique is viable and applicable to dispersive modes, the SSP method will be applied to synthesised signals with dispersive modes present. To simulate the propagation of the DWMs in time and space, the technique presented by Wilcox [14] can be employed. The frequency and wavenumber of the input signal are modified during the signal synthesis process, shifting the phase of the desired wave packet depending on the frequency. The wave modes can be reconstructed in the time domain at any distance by knowing the waveform at one location, in this example the input signal at the transmitting point, and the parameters of each wave mode's dispersion [73]. This phase shift depends on the phase velocity of the wave mode, which is a function of frequency and a value that can be extracted from the information presented in figure 4.1. The Fourier transform can then be used to represent the dispersive wave packet $g(t)$ in the frequency domain as follows:

$$G(\omega) = \int_{-\infty}^{\infty} g(t) e^{j\omega t} dx \tag{4.1}$$

where $\omega = 2\pi f$ is the angular frequency and f is the frequency. To find $g(t)$ at a certain distance $x = d$, a transfer function related to $g(t)$ at $x = 0$ for dispersion of a single dispersive wave mode can be used. The following expression represents the transfer function in question:

$$H(\omega) = e^{j\omega \frac{x}{v_{phase}(\omega)}} \tag{4.2}$$

where $v_{phase}(\omega)$ corresponds to the phase velocity of the given wave mode. The time domain signal $g(t)$ can then be calculated by employing the inverse FTT.

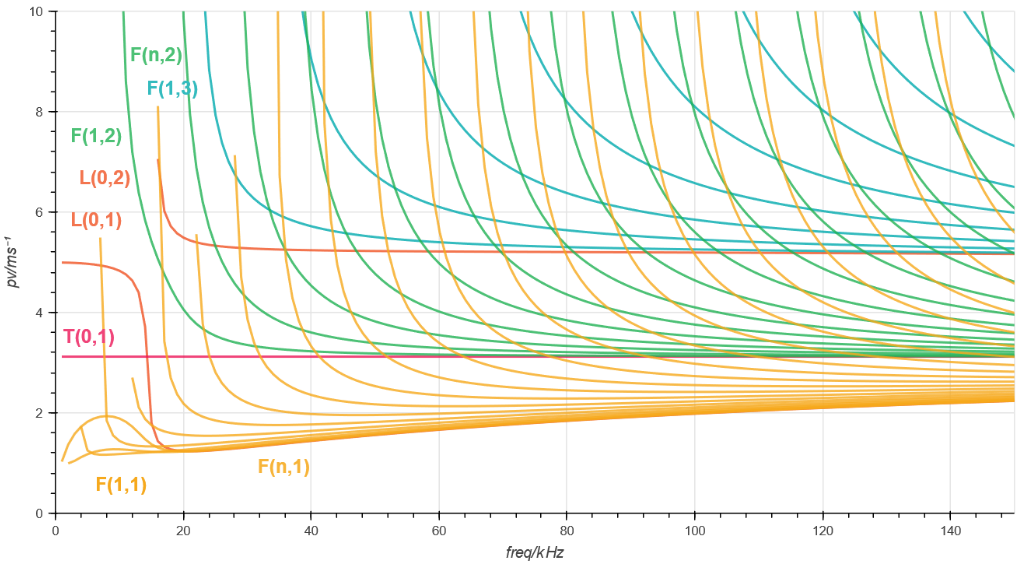

FIGURE 4.1: Phase velocity dispersion curves for a 4-inch steel pipe. The order n of the flexural modes increases from left to right.

While all of the velocities of the flexural wave modes are frequency dependent, the phase velocity of $T(0,1)$ is constant over the frequency bandwidth of interest. The order of each mode m goes up to three in Flexural wave modes, whereas the circumferential order can take various values. It should be noted that higher-order flexural wave modes exist as well, but because they are more dispersive, the first six orders used here are harder to eliminate.

A set of synthesised UGW signals is produced using the method previously mentioned. A 5-cycle Hann windowed sine pulse with a frequency of 60 kHz is shown in figure 4.2, which is utilised as the excitation signal. The *T(0,1)* and its family of flexural wave modes up to *F. (6,2)* is represented in figure 4.4 and finally, figure 4.5 depicts the total of the aforementioned wave modes.

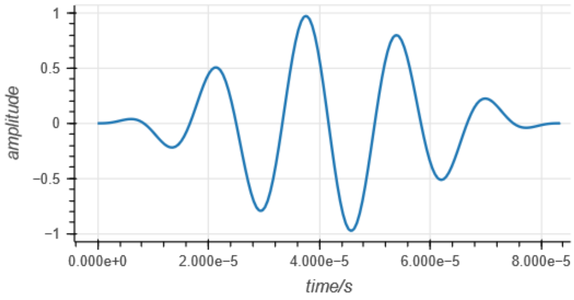

FIGURE 4.2: Excitation signal for a frequency of 60 kHz.

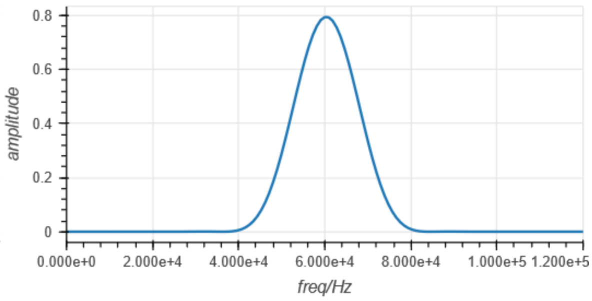

FIGURE 4.3: Frequency spectrum of the signal in figure 4.2.

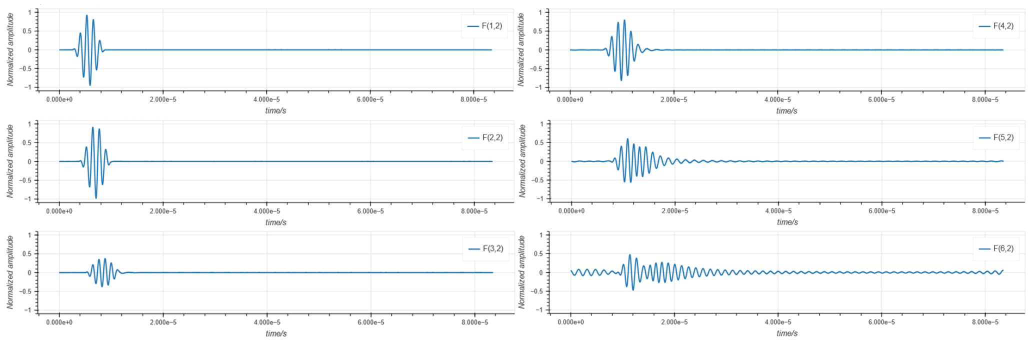

FIGURE 4.4: Synthesised UGW signals for dispersive Flexural *F(1,2)*, *F(2,2)*,...,*F(6,2)* wave modes family in a 4-inch steel pipe.

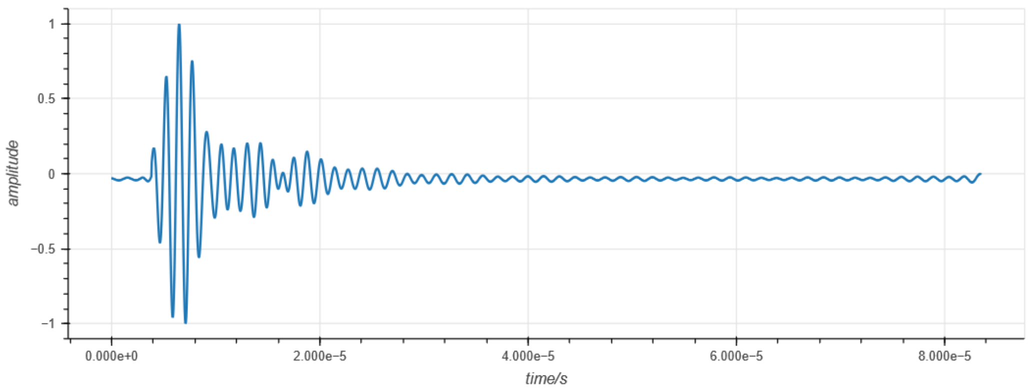

FIGURE 4.5: Time domain synthesised received UGW signal resulting from the combination of the signals above.

Other wave modes present in the signal can be taken into consideration as noise for approaches based on a single axisymmetric mode. The spatial resolution and SNR of the target axisymmetric wave mode, *T(0,1)*, are reduced by these dispersive modes. This artificial UGW signal is used to examine the SSP method by contrasting the various SSP recombination techniques.

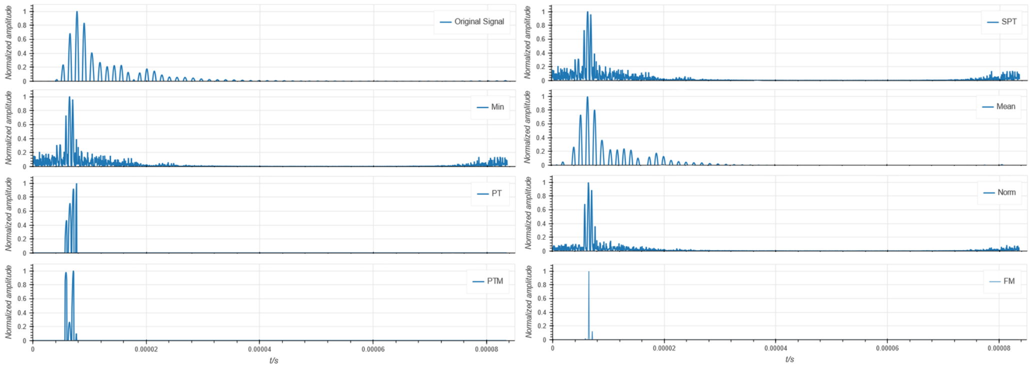

FIGURE 4.6: Results for the synthesised signals after applying the recombination algorithms.

The outputs from each SSP recombination algorithm show a dominant wave that arrives at the same time, but the amount of coherent noise resulting from the flexural wave modes varies for each algorithm. For most of the methods, some increase in the SNR can be observed. Figure 4.6 shows that the PT and PTM algorithms produce the maximum signal enhancement with the suggested parameters. In these situations, the spatial resolution is also superior.

Additionally, the SNR increase is calculated using equation 3.10 in order to evaluate the benefits demonstrated by the suggested technique, where S is the highest amplitude of the defect's reflection and N is the RMS value of the noise zone. The reference SNR value of the signal before employing any of the coherent noise filtering techniques is 30 dB. The SNR enhancement is obtained using equation 3.10. These values were all calculated for each of the recombination techniques and can be found in table 4.1.

SSP recombination algorithms	**SNR enhancement (dB)**
Minimisation	7.32
Polarity threshold	29.56
Polarity threshold with minimisation	22.83
Scaled polarity threshold	6.61
Mean	1.51
Normalisation	8.85
Frequency multiplication	11.73

TABLE 4.1: SNR enhancement values calculated for each recombination algorithm applied to synthesised signals.

It is important to note that the SNR enhancement is dependent on the input noise and dispersion levels and as a result, when the signal is less noisy or less dispersive, the performance of the other methods will be enhanced.

4.2 Experimental validation

To corroborate the technique studied and implemented to eliminate dispersive modes in UGWT signals and enhance the spatial resolution, the method has been applied to several signals obtained from laboratory experiments. These include signals obtained from the Pulse-echo technique and a Michelson interferometer of fibre with 1.5 *m* and 2 *cm* dimensions.

The pipe under study is a 4 inches diameter steel pipe of approximately 18 *m* in length with a wall thickness of 6.04 *mm*. The pipe presents several characteristics such as defects, welds and other features such as supports that affect the received signals. The location of these elements is represented in figure 4.7 which also includes the position of the different sensors used.

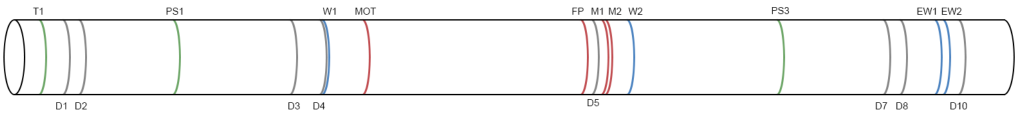

FIGURE 4.7: Illustration of the 4-inch steel pipe used for experimental validation, containing the location of the sensors (red), welds (blue), defects (grey), and other features (green).

To transmit the signal through the structure, a device called MOT (Magnetic Optical Transducer) is utilised. It was developed by EQS Global to assess the integrity of large areas in structures in service and consists of a transducer which combines the generation of ultrasound by magnetostriction, with the quasi-distributed detection by optical fibre sensors, allowing the evaluation of up to 100 meters in length and 360°. A Michelson Interferometer is then used to receive the signal. To produce a *T(0,1)* wave mode, the excitation pulse is transmitted along the pipe structure. The transducer (MOT) and Michelson interferometer (M1) positions are shown in figure 4.7 and the sampling rate was established at 2 *MHz*. As a result of their placement throughout the pipe's length, the received signal will include reflections from backwards propagation, making analysis more difficult.

Once the signals have been acquired, they will be processed following the procedure detailed in the previous chapter and the SSP technique will be implemented to filter the dispersive wave modes. Keeping in mind the results of the recombination algorithm, the original signals will be reconstructed based on these results, as described in the section below.

4.2.1 Signal reconstruction

Following the recombination, an attempt was made to reconstruct the original signal based on the results obtained from the recombination algorithms since the SSP results provide a representation of where in the signal the frequency remains constant, and not an actual representation of the signal itself. Since the best results have been obtained considering the polarity threshold recombination algorithms, these are the results that will be considered for the reconstruction.

The first attempt at signal reconstruction takes the results obtained from the recombination of sub-bands and eliminated the original signal where the results is null, leaving the signal unaltered where it is different from zero. The reconstructed signal is represented in figure 4.8.

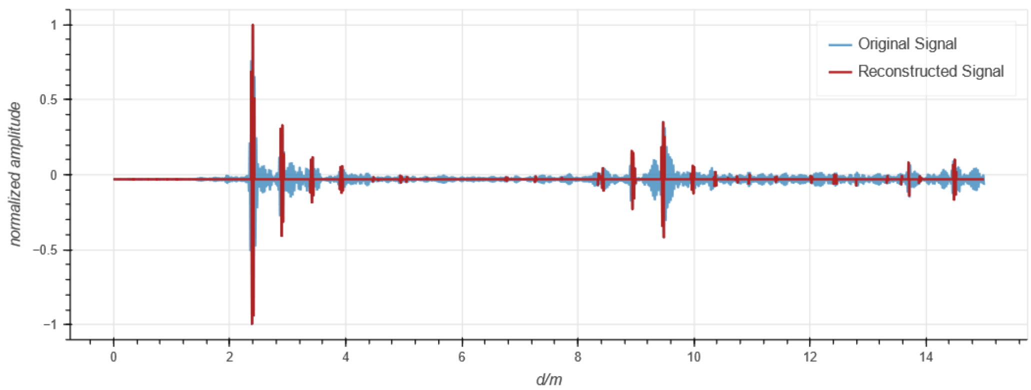

FIGURE 4.8: Representation of the reconstructed signal by eliminating the signal where the SSP recombination algorithm output is zero.

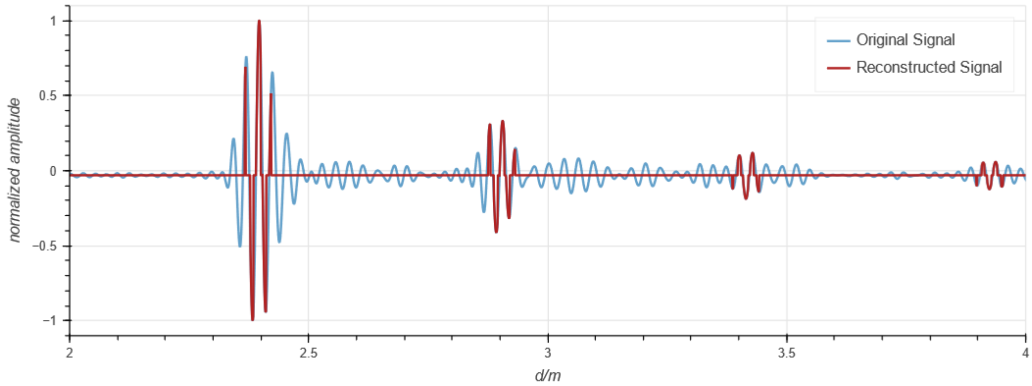

FIGURE 4.9: Zoom in figure of the signal represented in figure 4.8 between 2 m and 4 m.

The second attempt follows the first approach, but instead of eliminating the signal, the originally received data is attenuated by a coefficient of 0.1 where the recombination results are null. The reconstructed signal is represented in figure 4.10, providing an SNR enhancement of 37.66 dB.

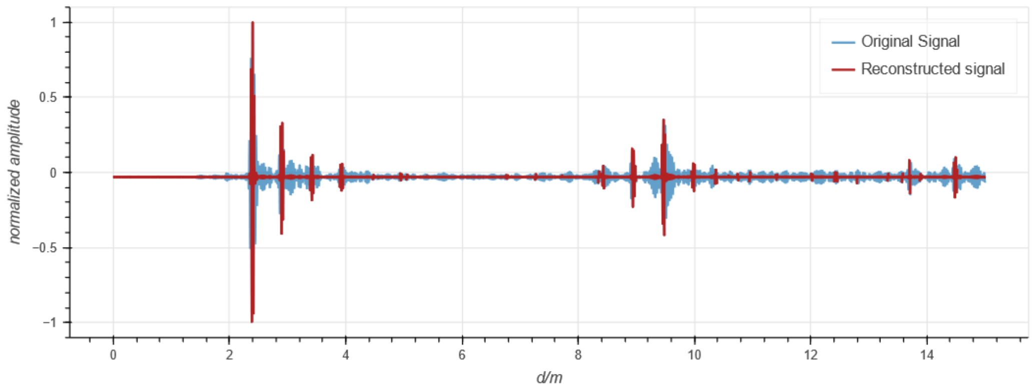

FIGURE 4.10: Representation of the reconstructed signal by attenuating the signal where the SSP recombination algorithm output is zero.

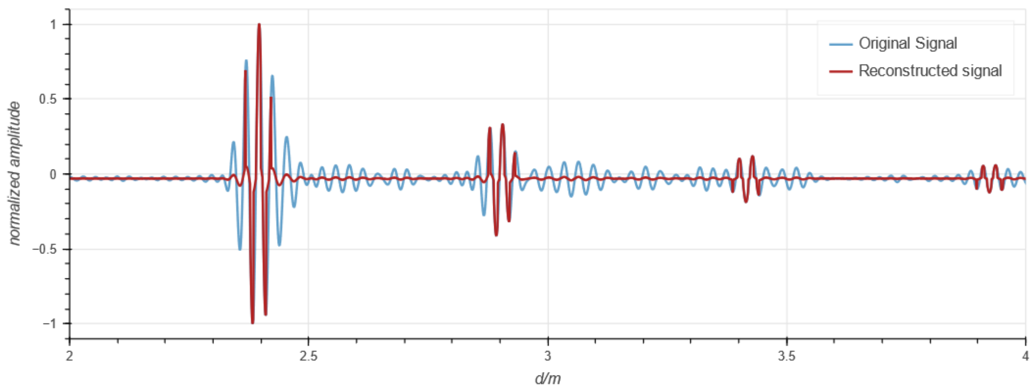

FIGURE 4.11: Zoom in figure of the signal represented in figure 4.10 between 2 m and 4 m.

The reconstructed signal obtained through the second method produces a result that is more accurate in comparison to the original signal, while still eliminating dispersive modes and highlighting the location of reflections resulting from defects, welds and other features.

4.2.2 Signal analysis

Two separate signals have been acquired: one with the pulse-echo technique, which presents very low dispersion levels and one with the Michelson interferometer which is highly dispersive. The first one will be used as a reference signal when analysing the defect locations and the performance of the SSP algorithm.

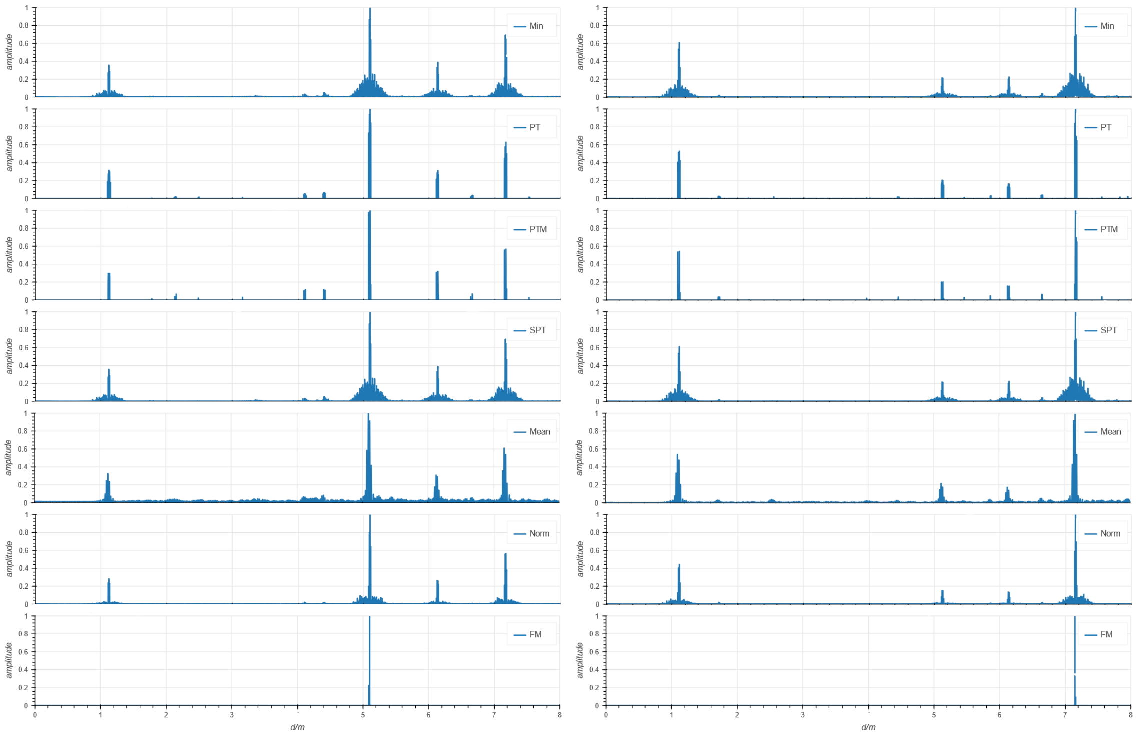

FIGURE 4.12: Results for recombination algorithms obtained from the pulse-echo technique signals for the left and right sides respectively.

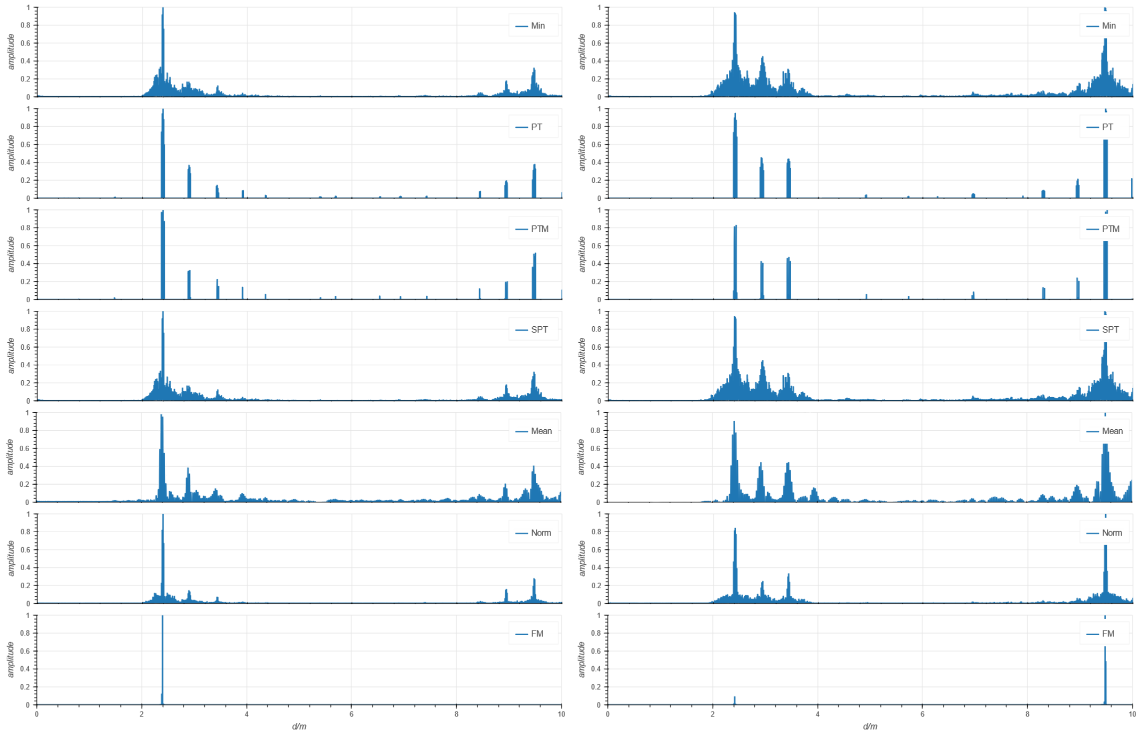

FIGURE 4.13: Results for recombination algorithms obtained from the Michelson interferometer technique signals for the left and right sides respectively.

In conformity with what was found in the previous section, the polarity threshold (PT) and polarity threshold with minimisation (PTM) algorithms provide the best results in terms of signal-to-noise enhancement and defect detection, resulting in an improvement of 37.86 dB and 35.64 dB, respectively. The SNR improvement values were calculated for the dispersive signals, meaning the ones acquired through the interferometer and the results are presented in table 4.2. On the other hand, the reflection signal from the defect has been eliminated by the FM algorithm, and therefore its SNR improvement cannot be measured. This distortion results from multiplying each sub-frequency bands without considering the signal's sign. PTM and PT are selected as the best SSP recombination algorithms for UGW data as a result.

SSP recombination algorithms	**SNR enhancement (dB)**
Minimisation	4.58
Polarity threshold	37.86
Polarity threshold with minimisation	35.64
Scaled polarity threshold	11.87
Mean	10.94
Normalisation	16.07

TABLE 4.2: SNR enhancement values calculated for each recombination algorithm applied to synthesised signals.

From the results obtained for the PT and PTM algorithms, the signal acquired were reconstructed following the method expressed in the previous section. Figures 4.14, 4.15, 4.16 and 4.17 represent the original input unprocessed signal superimposed with its reconstructed signal based on the result of the SSP recombination, as well as the location of the pipe's features. As the figures illustrates, there is often a shift from the signal's reflection and the true location of the defect or weld. This is due to mode conversion inside the pipe structure, which alters the velocity at which the signal travels along the material. In practical terms, although precision and accuracy are important and should be improved in future works, a shift equivalent to a few centimetres does not affect detection significantly.

The findings demonstrate that the unprocessed signal has a lower likelihood and degree of confidence in detecting the flaws since they are at a comparable level to the background coherent noise created by the presence of dispersive wave modes. In contrast, the suggested SSP approach, including PT and PTM recombination techniques, completely remove the noise and only the defect's reflection is left, with no artifacts or signal distortion. However, for defects of smaller cross-sectional area or location too close to other features such as welds, detection is still hard to achieve.

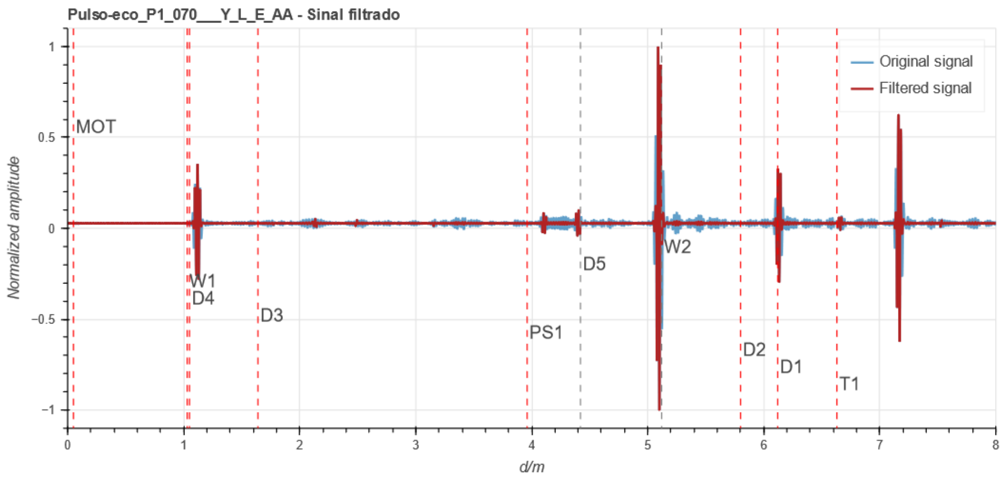

FIGURE 4.14: Input and reconstructed signal for the left side of the pulse-echo technique including the location of the pipe features.

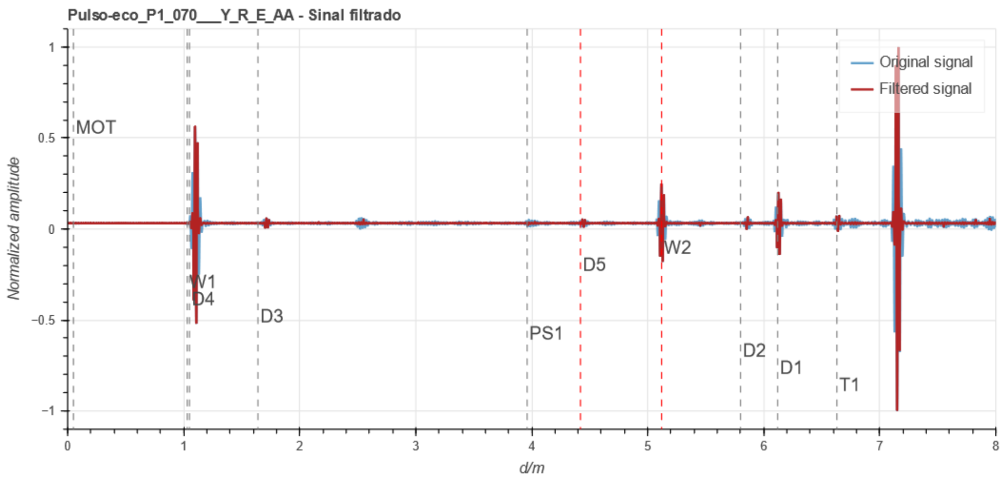

FIGURE 4.15: Input and reconstructed signal for the right side of the pulse-echo technique including the location of the pipe features.

The vertical dotted lines on the graphs (Figures 4.14, 4.15, 4.16, 4.17) represent the locations of the defects, welds and other features present in the pipe structure. The emission signals can be propagated to either side of the emission point, left or right. However, due to the effect of reflection, characteristics on the opposite side of the emission point can still be captured by the signal, not only from the opposite side but reflected echoes from the welds due to the multiple reflections. The grey lines correspond to the defects on the same side as the direction of propagation and the red lines to defects on the opposite side.

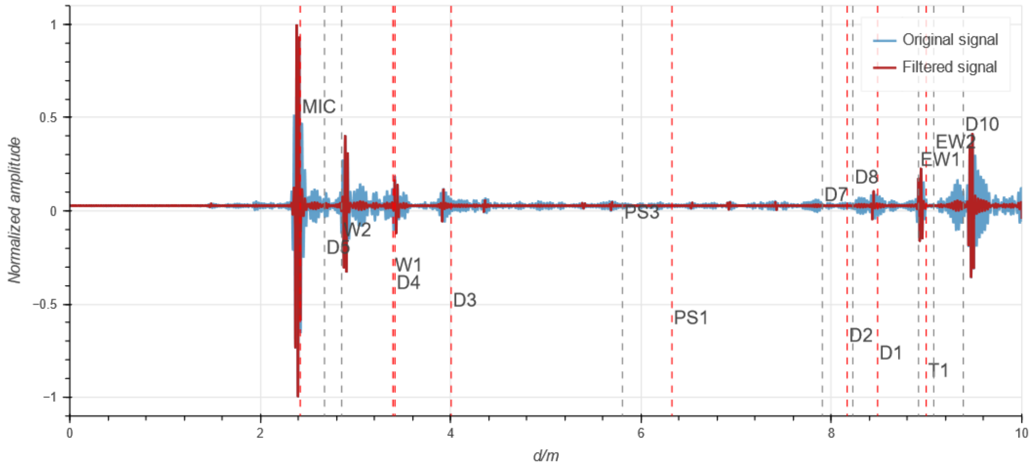

FIGURE 4.16: Input and reconstructed signal for the left side of the Michelson interferometer technique including the location of the pipe features.

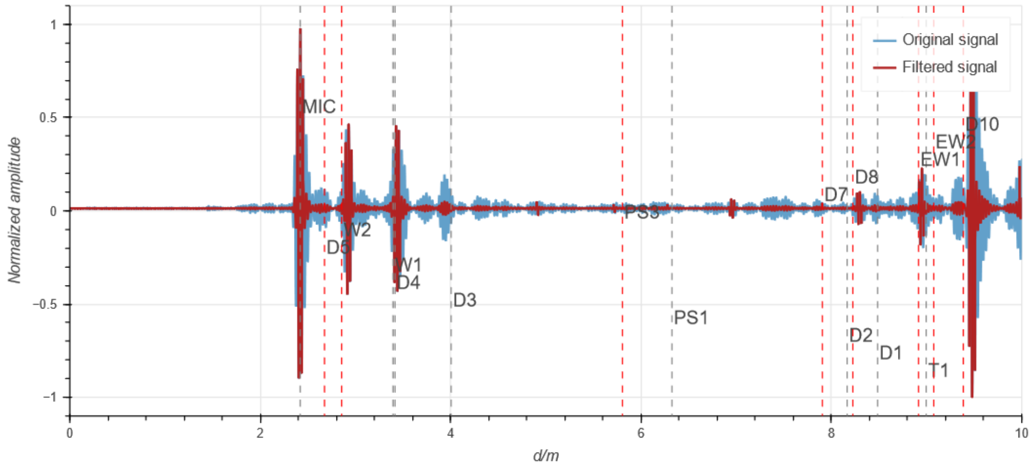

FIGURE 4.17: Input and reconstructed signal for the right side of the Michelson interferometer technique including the location of the pipe features.

The results of the experimental and synthesised signals demonstrate that the degree of coherent noise resulting from the existence of dispersive wave modes in ultrasonic guided wave signals may be greatly reduced by applying the SSP method. The SNR and spatial resolution of the signals can be significantly increased if coherent noise is properly decreased, which is frequently a major limiting factor for defect identification.

When compared to results obtained in previous works, it's important to mention that the outcome of the recombination algorithms presents a slight distortion in contrast with the original signal. On the other hand, the approach taken for the parameter selection for implementation results in a higher number of filters than most works use. The signals analysed throughout the internship were also obtained for longer distances (between 10 and 14 m as opposed to 2 and 6 m) and contained a higher number of defects, some very close to each other, which makes their analysis more complex and defect detection harder to achieve.

Chapter 5

Conclusion

5.1 Conclusions

In the context of the health and integrity of industry infrastructure, ultrasonic guided wave testing has been one of the main methods to perform surveillance and monitoring and large structural components for defects. The detection of these faults is essential since the failure of these structures can lead to high economic losses, both directly from unforeseen stops and indirectly via supply problems. However, the dispersion present in UGWT signals makes their analysis more complex and thus makes the detection of flaws harder to achieve. The work developed throughout this internship has had the aim to reduce the effect of dispersion and improvement of SNR in acquired signals by implementing an advanced signal processing algorithm, to improve data analysis for UGWT using magnetostrictive transducers.

To first learn about the topic, a state-of-the-art literature review was done, where different techniques for signal processing, applied to structures such as plates and pipes, were compared to choose the best option in terms of advantages and complexity. The technique chosen was Split Spectrum Processing, for its simplicity of implementation and good results obtained in previous works for SNR improvement. The key issue with this method is the choice of parameters for the bank filter, as the performance of the SSP algorithm is highly sensitive to the variation of said parameters. By testing the SNR and spatial resolution of the received signals, the brute force search algorithm was used to identify the best values for these parameters. For the pipe structure and signals studied, the optimum values obtained were B = 90% of the total operation frequency, $B_{filt} = B/7$

and $F = B_{filt}/4.5$. If the structure or conditions change, the optimum parameters also need to be changed.

The parameters were then defined through search brute force and comparing results for different signals at different frequencies. The SSP method was applied to both synthesised and experimental data. The proposed parameters have been tested for *T(0,1)* wave mode and its flexural wave modes family up to *F(6,2)*. Once the parameters had been defined, the SSP method was applied to both synthesised and experimental data. The proposed parameters have been tested for *T(0,1)* wave mode and its flexural wave modes family up to *F(6,2)*. For the synthesised signals, the best results were achieved for the PT and PTM recombination algorithms, with SNR improvements of 29 dB and 23 dB. For the experimental signals, the same recombination methods were found to provide the best results, with values of SNR improvements of 38 dB and 36 dB, respectively. The experimental findings supported the claim that the suggested approach significantly lowers the level of dispersive wave mods in the UGWT signal response.

5.2 Future work

Further work on this subject should focus on the improvement of the selection of the optimum bank filter parameters and testing on more field data under various conditions and defects. As explained throughout the report, the optimum parameters take on different values depending on the material, geometry and dimensions of the structure under inspection, due to the change of dispersion curves based on the characteristics of the structure. Even though the parameters can be reutilised for structures with similar properties, the selection process is currently done through brute search force algorithm, which is arduous and time consuming. The introduction of machine learning technology to optimise and automise the selection process, therefore would greatly improve these methods and make the implementation of this algorithm more efficient and straightforward. On the other hand, it would be of great interest as well to reconstruct the signal of the dispersive modes rather than eliminate them altogether to obtain more detailed information on the integrity of the structure.

Bibliography

[1] J. L. Rose, *Ultrasonic guided waves in solid media*. Cambridge university press, 2014. [Cited on pages 1 and 2.]

[2] A. R. Diogo, B. Moreira, C. A. J. Gouveia, and J. M. R. S. Tavares, "A review of signal processing techniques for ultrasonic guided wave testing," *Metals*, vol. 12, no. 6, 2022. [Online]. Available: https://www.mdpi.com/2075-4701/12/6/936 [Cited on pages xi and 2.]

[3] P. Cawley, M. Lowe, D. Alleyne, B. Pavlakovic, and P. Wilcox, "Practical long range guided wave inspection-applications to pipes and rail," *Mater. Eval*, vol. 61, no. 1, pp. 66–74, 2003. [Cited on pages 2 and 4.]

[4] P. Wilcox, M. Lowe, and P. Cawley, "The effect of dispersion on long-range inspection using ultrasonic guided waves," *Ndt & E International*, vol. 34, no. 1, pp. 1–9, 2001. [Cited on page 3.]

[5] S. Liu, J. Ding, and S. Wang, "Application of ultrasonic guided wave testing for overhead pipelines in service," *American Society of Mechanical Engineers, Pressure Vessels and Piping Division (Publication) PVP*, vol. 5, 2021. [Cited on pages 4, 11, and 14.]

[6] H. Mahal, K. Yang, and A. Nandi, "Defect detection using power spectrum of torsional waves in guided-wave inspection of pipelines," *Applied Sciences (Switzerland)*, vol. 9, 2019. [Cited on pages 12 and 14.]

[7] J. Rostami, P. Tse, and Z. Fang, "Sparse and dispersion-based matching pursuit for minimizing the dispersion effect occurring when using guidedwave for pipe inspection," *Materials*, vol. 10, 2017. [Cited on pages 4, 8, 12, and 14.]

[8] N. E. Huang, Z. Shen, S. R. Long, M. C. Wu, H. H. Shih, Q. Zheng, N.-C. Yen, C. C. Tung, and H. H. Liu, "The empirical mode decomposition and the hilbert spectrum

for nonlinear and non-stationary time series analysis," *Proceedings: Mathematical, Physical and Engineering Sciences*, vol. 454, no. 1971, pp. 903–995, 1998. [Online]. Available: http://www.jstor.org/stable/53161 [Cited on page 5.]

[9] W. Prosser, M. Seale, and B. Smith, "Time-frequency analysis of the dispersion of lamb modes," *The Journal of the Acoustical Society of America*, vol. 105, 01 2000. [Cited on page 17.]

[10] M. Niethammer, L. J. Jacobs, J. Qu, and J. Jarzynski, "Time-frequency representations of lamb waves," *The Journal of the Acoustical Society of America*, vol. 109, no. 5, pp. 1841–1847, 2001. [Online]. Available: https://doi.org/10.1121/1.1357813 [Cited on page 17.]

[11] B. Wu, F. Deng, and C.-F. He, "Review of signal processing in ultrasonic guided waves nondestructive testing," *Beijing Gongye Daxue Xuebao / Journal of Beijing University of Technology*, vol. 33, pp. 342–348, 2007.

[12] B. Lu, B. Upadhyaya, and R. Perez, "Structural integrity monitoring of steam generator tubing using transient acoustic signal analysis," *IEEE Transactions on Nuclear Science*, vol. 52, pp. 484–493, 2005. [Cited on page 5.]

[13] C. Valle and J. L. Jr., "Flaw localization using the reassigned spectrogram on laser-generated and detected lamb modes," *Ultrasonics*, vol. 39, pp. 535–542, 2002. [Cited on page 8.]

[14] P. Wilcox, "A rapid signal processing technique to remove the effect of dispersion from guided wave signals," *IEEE Transactions on Ultrasonics, Ferroelectrics, and Frequency Control*, vol. 50, pp. 419–427, 2003. [Cited on page 49.]

[15] M. Silva, R. Gouyon, and F. Lepoutre, "Hidden corrosion detection in aircraft aluminum structures using laser ultrasonics and wavelet transform signal analysis," *Ultrasonics*, vol. 41, pp. 301–305, 2003.

[16] X. Li, X.-B. Li, and L. Chen, "Study of ultrasonic guided waves signal based on morphology component analysis method," *Tien Tzu Hsueh Pao/Acta Electronica Sinica*, vol. 41, pp. 444–450, 2013. [Cited on page 8.]

[17] J. Moll, C. Heftrich, and C.-P. Fritzen, “Time-varying inverse filtering of narrowband ultrasonic signals,” *Structural Health Monitoring*, vol. 10, pp. 403–415, 2011. [Cited on page 8.]

[18] A. Demma, P. Cawley, M. Lowe, and A. G. Roosenbrand, “The reflection of the fundamental torsional mode from cracks and notches in pipes,” *The Journal of the Acoustical Society of America*, vol. 114, no. 2, pp. 611–625, 2003. [Online]. Available: https://doi.org/10.1121/1.1582439 [Cited on page 8.]

[19] J. Wu, X. Chen, and Z. Ma, “A signal decomposition method for ultrasonic guided wave generated from debonding combining smoothed pseudo wigner-ville distribution and vold-kalman filter order tracking,” *Shock and Vibration*, vol. 2017, 2017. [Cited on pages 8, 17, and 21.]

[20] J. Grabowska, M. Palacz, and M. Krawczuk, “Damage identification by wavelet analysis,” *Mechanical Systems and Signal Processing*, vol. 22, pp. 1623–1635, 2008. [Cited on pages 8 and 11.]

[21] P. Catton, P. Mudge, and W. Balachandran, “Advances in defect characterisation using long-range ultrasonic testing of pipes,” *Insight: Non-Destructive Testing and Condition Monitoring*, vol. 50, pp. 480–484, 2008.

[22] J.-H. Lee and S.-J. Lee, “Application of laser-generated guided wave for evaluation of corrosion in carbon steel pipe,” *NDT and E International*, vol. 42, pp. 222–227, 2009.

[23] R. Levine and J. Michaels, “Model-based imaging of damage with lamb waves via sparse reconstruction,” *Journal of the Acoustical Society of America*, vol. 133, pp. 1525–1534, 2013.

[24] C. Li, Y. Wang, L. Zhu, and C. Shen, “Application of improved matching pursuit method in guided wave signal processing,” *Zhendong Ceshi Yu Zhenduan/Journal of Vibration, Measurement and Diagnosis*, vol. 32, pp. 111–115, 2012. [Cited on pages 8 and 11.]

[25] F. Cau, A. Fanni, A. Montisci, P. Testoni, and M. Usai, “A signal-processing tool for non-destructive testing of inaccessible pipes,” *Engineering Applications of Artificial Intelligence*, vol. 19, pp. 753–760, 2006. [Cited on pages 8 and 13.]

[26] P. Gardner, R. Fuentes, N. Dervilis, C. Mineo, S. Pierce, E. Cross, and K. Worden, "Machine learning at the interface of structural health monitoring and non-destructive evaluation: Machine learning in shm and nde," *Philosophical Transactions of the Royal Society A: Mathematical, Physical and Engineering Sciences*, vol. 378, 2020. [Cited on page 8.]

[27] B. Liu, L. Tang, J. Wang, A. Li, and Y. Hao, "2-d defect profile reconstruction from ultrasonic guided wave signals based on qga-kernelized elm," *Neurocomputing*, vol. 128, pp. 217–223, 2014. [Cited on page 8.]

[28] W. Zhang, H. Hao, J. Wu, J. Li, H. Ma, and C. Li, "Detection of minor damage in structures with guided wave signals and nonlinear oscillator," *Measurement*, vol. 122, 07 2017. [Cited on page 8.]

[29] B. Widrow, J. Glover, J. McCool, J. Kaunitz, C. Williams, R. Hearn, J. Zeidler, J. Eugene Dong, and R. Goodlin, "Adaptive noise cancelling: Principles and applications," *Proceedings of the IEEE*, vol. 63, no. 12, pp. 1692–1716, 1975. [Cited on page 9.]

[30] H. Mahal, K. Yang, and A. Nandi, "Improved defect detection using adaptive leaky nlms filter in guided-wave testing of pipelines," *Applied Sciences (Switzerland)*, vol. 9, 2019. [Cited on pages xi, 9, 10, and 15.]

[31] E. W. Beasley and H. R. Ward, "A quantitative analysis of sea clutter decorrelation with frequency agility," *IEEE Transactions on Aerospace and Electronic Systems*, vol. AES-4, pp. 468–473, 1968. [Cited on page 10.]

[32] V. L. Newhouse, N. M. Bilgutay, J. Saniie, and E. S. Furgason, "Flaw-to-grain echo enhancement by split-spectrum processing," *Ultrasonics*, vol. 20, pp. 59–68, 1982. [Cited on page 10.]

[33] S. Pedram, S. Fateri, L. Gan, A. Haig, and K. Thornicroft, "Split-spectrum processing technique for snr enhancement of ultrasonic guided wave," *Ultrasonics*, vol. 83, pp. 48–59, 2018. [Cited on pages 10 and 14.]

[34] S. Pedram, T.-H. Gan, and M. Ghafourian, "Improved defect detection of guided wave testing using split-spectrum processing," *Sensors (Switzerland)*, vol. 20, pp. 1–18, 2020. [Cited on pages 10 and 15.]

[35] H. Mahal, K. Yang, and A. Nandi, "Detection of defects using spatial variances of guided-wave modes in testing of pipes," *Applied Sciences (Switzerland)*, vol. 8, 2018. [Cited on pages 11 and 15.]

[36] A. Haar, "Zur theorie der orthogonalen funktionensysteme," *Mathematische Annalen*, vol. 69, no. 3, pp. 331–371, 09 1910. [Cited on page 11.]

[37] J. Chen, J. Rostami, P. Tse, and X. Wan, "The design of a novel mother wavelet that is tailor-made for continuous wavelet transform in extracting defect-related features from reflected guided wave signals," *Measurement: Journal of the International Measurement Confederation*, vol. 110, pp. 176–191, 2017. [Cited on pages 11 and 14.]

[38] S. Mallat and Z. Zhang, "Matching pursuits with time-frequency dictionaries," *IEEE Transactions on Signal Processing*, vol. 41, no. 12, pp. 3397–3415, 1993. [Cited on page 11.]

[39] E. Wigner, "On the quantum correction for thermodynamic equilibrium," *Phys. Rev.*, vol. 40, pp. 749–759, Jun 1932. [Online]. Available: https://link.aps.org/doi/10.1103/PhysRev.40.749 [Cited on page 12.]

[40] S. Majhi, A. Mukherjee, N. George, and B. Uy, "Corrosion detection in steel bar: A time-frequency approach," *NDT and E International*, vol. 107, 2019. [Cited on pages 13 and 15.]

[41] T. Di Ianni, L. De Marchi, A. Perelli, and A. Marzani, "Compressive sensing of full wave field data for structural health monitoring applications," *Ultrasonics, Ferroelectrics, and Frequency Control, IEEE Transactions on*, vol. 62, pp. 1373–1383, 07 2015. [Cited on page 16.]

[42] Y. Da, B. Wang, and Z. Qian, "Noise processing of flaw reconstruction by wavelet transform in ultrasonic guided sh waves," *Meccanica*, vol. 52, pp. 2307–2328, 2017. [Cited on pages 16 and 21.]

[43] P. Zabbal, G. Ribay, B. Chapuis, and J. Jumel, "Multichannel multiple signal classification for dispersion curves extraction of ultrasonic guided waves," *The Journal of the Acoustical Society of America*, vol. 143, no. 2, pp. EL87–EL92, 2018. [Online]. Available: https://doi.org/10.1121/1.5022699 [Cited on page 16.]

[44] K. Xu, J.-G. Minonzio, D. Ta, B. Hu, W. Wang, and P. Laugier, "Sparse svd method for high resolution extraction of the dispersion curves of ultrasonic guided waves," *IEEE Transactions on Ultrasonics Ferroelectrics and Frequency Control*, vol. 63, 07 2016. [Cited on page 16.]

[45] Q. Chen, K. Xu, and D. Ta, "High-resolution lamb waves dispersion curves estimation and elastic property inversion," *Ultrasonics*, vol. 115, 2021. [Cited on pages 16 and 21.]

[46] S. Sabeti and J. Harley, "Spatio-temporal undersampling: Recovering ultrasonic guided wavefields from incomplete data with compressive sensing," *Mechanical Systems and Signal Processing*, vol. 140, 2020. [Cited on pages 17 and 21.]

[47] M. Ratassepp and Z. Fan, "Wave mode extraction from multimodal guided wave signal in a plate," *AIP Conference Proceedings*, vol. 1706, no. 1, p. 030012, 2016. [Online]. Available: https://aip.scitation.org/doi/abs/10.1063/1.4940484 [Cited on page 18.]

[48] S. Rizvi and M. Abbas, "An advanced wigner-ville time-frequency analysis of lamb wave signals based upon an autoregressive model for efficient damage inspection," *Measurement Science and Technology*, vol. 32, 2021. [Cited on pages 18 and 22.]

[49] A. Bagheri and P. Rizzo, "Guided ultrasonic wave testing of an immersed plate with hidden defects," *Optical Engineering*, vol. 55, 2016. [Cited on pages 18 and 22.]

[50] H. Jia, H. Liu, Z. Zhang, F. Dai, Y. Liu, and J. Leng, "A baseline-free approach of locating defect based on mode conversion and the reciprocity principle of lamb waves," *Ultrasonics*, vol. 102, 2020. [Cited on pages 18 and 22.]

[51] G. Wang, Y. Wang, H. Sun, B. Miao, and Y. Wang, "A reference matching-based temperature compensation method for ultrasonic guided wave signals," *Sensors (Switzerland)*, vol. 19, 2019. [Cited on page 22.]

[52] A. Douglass and J. Harley, "Dynamic time warping temperature compensation for guided wave structural health monitoring," *IEEE Transactions on Ultrasonics, Ferroelectrics, and Frequency Control*, vol. 65, pp. 851–861, 2018. [Cited on pages 18 and 22.]

[53] V. Ewald, R. S. Venkat, A. Asokkumar, R. Benedictus, C. Boller, and R. Groves, "Perception modelling by invariant representation of deep learning for automated structural diagnostic in aircraft maintenance: A study case using deepshm," *Mechanical Systems and Signal Processing*, vol. 165, 2022. [Cited on page 18.]

[54] J. He, C. A. Leckey, P. E. Leser, and W. P. Leser, "Multi-mode reverse time migration damage imaging using ultrasonic guided waves," *Ultrasonics*, vol. 94, pp. 319–331, 2019. [Online]. Available: https://www.sciencedirect.com/science/article/pii/S0041624X18303846 [Cited on pages 18 and 23.]

[55] T. Hay, R. Royer, H. Gao, X. Zhao, and J. Rose, "A comparison of embedded sensor lamb wave ultrasonic tomography approaches for material loss detection," *Smart Materials and Structures*, vol. 15, p. 946, 06 2006. [Cited on page 18.]

[56] Y. Lee and Y. Cho, "Defect imaging enhancement through optimized shape factors of the rapid algorithm based on guided wave beam pattern analysis," *Sensors*, vol. 21, 2021. [Cited on pages xi, 19, and 23.]

[57] C.-B. Xu, Z.-B. Yang, Z. Zhai, B.-J. Qiao, S.-H. Tian, and X.-F. Chen, "A weighted sparse reconstruction-based ultrasonic guided wave anomaly imaging method for composite laminates," *Composite Structures*, vol. 209, pp. 233–241, 2019. [Cited on pages 19 and 23.]

[58] H.-Y. Zhang, J. Yang, G.-P. Fan, W.-F. Zhu, and X.-D. Chai, "Reverse time migration lamb wave imaging based on mode separation," *Wuli Xuebao/Acta Physica Sinica*, vol. 66, 2017. [Cited on pages 19 and 23.]

[59] J. Rao, M. Ratassepp, and Z. Fan, "Investigation of the reconstruction accuracy of guided wave tomography using full waveform inversion," *Journal of Sound and Vibration*, vol. 400, pp. 317–328, 2017. [Online]. Available: https://www.sciencedirect.com/science/article/pii/S0022460X17303231 [Cited on page 19.]

[60] Y. Lugovtsova, J. Bulling, O. Mesnil, J. Prager, D. Gohlke, and C. Boller, "Damage quantification in an aluminium-cfrp composite structure using guided wave wavenumber mapping: Comparison of instantaneous and local wavenumber analyses," *NDT and E International*, vol. 122, 2021. [Cited on pages 20 and 23.]

[61] K. Tiwari and R. Raisutis, "Identification and characterization of defects in glass fiber reinforced plastic by refining the guided lamb waves," *Materials*, vol. 11, 2018. [Cited on pages 20 and 24.]

[62] C. G. Muñoz, A. A. Jiménez, and F. G. Márquez, "Wavelet transforms and pattern recognition on ultrasonic guides waves for frozen surface state diagnosis," *Renewable Energy*, vol. 116, pp. 42–54, 2018. [Cited on pages 20 and 24.]

[63] A. A. Jiménez, C. G. Muñoz, and F. G. Márquez, "Dirt and mud detection and diagnosis on a wind turbine blade employing guided waves and supervised learning classifiers," *Reliability Engineering and System Safety*, vol. 184, pp. 2–12, 2019. [Cited on pages 20 and 24.]

[64] C.-B. Xu, Z.-B. Yang, X.-F. Chen, S.-H. Tian, and Y. Xie, "A guided wave dispersion compensation method based on compressed sensing," *Mechanical Systems and Signal Processing*, vol. 103, pp. 89–104, 2018. [Cited on pages 20 and 21.]

[65] K. Tiwari, R. Raisutis, and V. Samaitis, "Hybrid signal processing technique to improve the defect estimation in ultrasonic non-destructive testing of composite structures," *Sensors (Switzerland)*, vol. 17, 2017. [Cited on page 24.]

[66] C. He, S. Liu, Z. Liu, Y. Zhang, and B. Wu, "Application of wavelet denoise in defect inspection of steel strands," *Jixie Gongcheng Xuebao/Chinese Journal of Mechanical Engineering*, vol. 44, pp. 118–122, 2008. [Cited on pages 25 and 26.]

[67] M. Legg, M. K. Yücel, V. Kappatos, C. Selcuk, and T.-H. Gan, "Increased range of ultrasonic guided wave testing of overhead transmission line cables using dispersion compensation," *Ultrasonics*, vol. 62, pp. 35–45, 2015. [Online]. Available: https://www.sciencedirect.com/science/article/pii/S0041624X15001018 [Cited on pages 25 and 26.]

[68] Q. Ji, L. Jian-Bin, L. Fan-Rui, Z. Jian-Ting, and W. Xu, "Stress evaluation in seven-wire strands based on singular value feature of ultrasonic guided waves," *Structural Health Monitoring*, 2021. [Cited on pages 25 and 27.]

[69] D. Tran, J.-W. Kim, K. Tola, W. Kim, and S. Park, "Artificial intelligence-based bolt loosening diagnosis using deep learning algorithms for laser ultrasonic wave propagation data," *Sensors (Switzerland)*, vol. 20, pp. 1–25, 2020. [Cited on pages 25 and 27.]

[70] C. Liew and M. Veidt, "Guided waves damage identification in beams with test pattern dependent series neural network systems," *WSEAS Transactions on Signal Processing*, vol. 4, pp. 86–96, 2008. [Cited on pages 26 and 27.]

[71] T. Ju and A. Findikoglu, "Large area detection of microstructural defects with multi-mode ultrasonic signals," *Applied Sciences (Switzerland)*, vol. 12, 2022. [Cited on pages 26 and 27.]

[72] X. Niu, H.-P. Chen, and H. Marques, "Piezoelectric transducer array optimization through simulation techniques for guided wave testing of cylindrical structures," 06 2017. [Cited on pages xi and 30.]

[73] B. Hernandez Crespo, C. R. P. Courtney, and B. Engineer, "Calculation of guided wave dispersion characteristics using a three-transducer measurement system," *Applied Sciences*, vol. 8, no. 8, 2018. [Online]. Available: https://www.mdpi.com/2076-3417/8/8/1253 [Cited on page 49.]